

RING-CPD: Asymptotic Distribution-free Change-point Detection for Multivariate and Non-Euclidean Data

Doudou Zhou and Hao Chen

Department of Statistics, University of California, Davis

Abstract: Change-point detection (CPD) concerns detecting distributional changes in a sequence of independent observations. Among nonparametric methods, rank-based methods are attractive due to their robustness and efficiency and have been extensively studied for univariate data. However, they are not well explored for high-dimensional or non-Euclidean data. In this paper, we propose a new method, Rank INduced by Graph Change-Point Detection (RING-CPD), based on graph-induced ranks to handle high-dimensional and non-Euclidean data. The new method is asymptotically distribution-free under the null hypothesis with an analytic p -value approximation derived for fast type-I error control. Extensive simulation studies show that the RING-CPD method works well for a wide range of alternatives and is robust to heavy-tailed distribution or outliers. The new method is illustrated by the detection of seizures in a functional connectivity network dataset and travel pattern changes in the New York City Taxi dataset.

Keywords and phrases: graph-induced ranks; tail probability; high-dimensional data; network data.

1. Introduction

Given a sequence of independent observations, an important problem is to decide whether the observations are from the same distribution or there is a change of distribution at a certain time point. Change-point detection (CPD) has attracted a lot of interests since the seminal work of [Page \(1954\)](#). In this big data era, it has diverse applications in many fields, including functional magnetic resonance recordings ([Barnett and Onnela, 2016](#); [Zambon, Alippi and Livi, 2019](#)), healthcare ([Staudacher et al., 2005](#); [Malladi, Kalamangalam and Aazhang, 2013](#)), communication network evolution ([Kossinets and Watts, 2006](#); [Eagle, Pentland and Lazer, 2009](#); [Peel and Clauset, 2015](#)), and financial modeling ([Bai and Perron, 1998](#); [Talih and Hengartner, 2005](#)). Parametric approaches (see for example [Srivastava and Worsley, 1986](#); [Zhang et al., 2010](#); [Siegmund, Yakir and Zhang, 2011](#); [Chen and Gupta, 2012](#); [Wang, Zou and Yin, 2018](#)) are useful to address the problem for univariate and low-dimensional data, however, they are limited for high-dimensional or non-Euclidean data due to a large number of parameters to be estimated unless very strong assumptions are imposed.

A few nonparametric methods have been proposed, including kernel-based methods (Desobry, Davy and Doncarli, 2005; Li et al., 2015; Garreau and Arlot, 2018; Arlot, Celisse and Harchaoui, 2019; Chang et al., 2019), interpoint distance-based methods (Matteson and James, 2014; Li, 2020) and graph-based methods (Chen and Zhang, 2015; Shi, Wu and Rao, 2017; Zhang and Chen, 2017; Chu and Chen, 2019; Chen, 2019; Song and Chen, 2020; Liu and Chen, 2020; Nie and Nicolae, 2021). However, many existing kernel-based and distance-based methods suffered from the curse of dimensionality for high-dimensional data (Chen and Friedman, 2017), thus losing power for some common types of changes. With the observation, Li (2020) proposed an asymptotic distribution-free approach utilizing all interpoint distances under the high dimension, low sample size setting. Their method worked well for detecting both location and scale changes. However, their test statistics are time-consuming and memory-consuming to construct, causing the method not applicable to large datasets. Also, the method implicitly requires the existence of the second moment of the underlying distribution, which can be violated by heavy-tailed data or outliers that are common in many applications. The graph-based CPD methods are promising approaches due to their flexibility and efficiency in analyzing high-dimensional and non-Euclidean data, with good performance for various changes. Chen and Zhang (2015) proposed the graph-based test that can be applied to generic graphs with analytical p -value approximations for type I error control, then Chu and Chen (2019) proposed new test statistics that take the curse of dimensionality into account and can detect various types of changes. However, the graph-based methods focused on unweighted graphs, which may cause information loss.

Among the nonparametric methods, rank-based methods are attractive due to their robustness and efficiency. For univariate data, rank tests for CPD have been extensively studied (Bhattacharyya and Johnson, 1968; Darkhovskh, 1976; Pettitt, 1979; Schechtman, 1982; Lombard, 1987, 1983; Gerstenberger, 2018; Wang, Wang and Zi, 2020). However, they are less explored for high-dimensional or non-Euclidean data. Specifically, existing multivariate rank-based methods do not apply to high-dimensional data with general changes. For instance, Lung-Yut-Fong, Lévy-Leduc and Cappé (2015) proposed to use the component-wise rank, which worked only when the dimension of the data is smaller than the number of observations. Zhang, Chen and Wu (2020) and Shu et al. (2022) proposed the spatial rank-based methods, which were designed mainly for the shift in the mean. Chenouri, Mozaffari and Rice (2020) proposed to use the ranks obtained from data depths, which is often used for low-dimensional data and is computation-extensive when the dimension is high.

Noticing the gap between the potential benefit of the rank-based method and the scarce exploration for multivariate/high-dimensional data, we propose a new rank-based method called Rank INduced by Graph Change-Point Detection (RING-CPD), which can be applied to high-dimensional and non-Euclidean data. Unlike previous works dealing with the ranks of observations that are often limited to low-dimensional distributions, we propose to use the rank induced by similarity graphs. Inspired by the recently developed graph-induced rank using

similarity graphs for the two-sample test problem (Zhou and Chen, 2021), we extend it to the CPD framework. The graph-induced rank is the rank defined in the similarity graphs. Instead of treating all edges in the graph equally, we assign the rank as weights to each edge and construct the scan statistics based on the ranks. For example, if the k -nearest neighbor graph (k -NNG) (Schilling, 1986; Henze, 1988) is used, the edges in the j th-NNG will be assigned the rank $k - j + 1$ for $j = 1, \dots, k$. More discussions on this rank and the new test are presented in Section 2. We prove that the proposed scan statistics are asymptotic distribution-free. They are also consistent against all types of changes when some special similarity graphs are used (Section 3). The proposed statistics can work for a wide range of alternatives. Specifically, they are robust to heavy-tailed distribution or outliers, as illustrated by extensive simulation studies in Section 4 and two real data examples in Section 5. The details of proofs of the theorems are deferred to Supplementary Material.

2. Method

For a sequence of independent observations $\{y_i\}_{i=1}^n$, we consider testing

$$H_0 : y_i \sim F_0, \quad i = 1, \dots, n$$

against the single change-point alternative

$$H_1 : \exists 1 \leq \tau < n, y_i \sim \begin{cases} F_0, & i \leq \tau \\ F_1, & \text{otherwise} \end{cases}$$

or the changed interval alternative

$$H_2 : \exists 1 \leq \tau_1 < \tau_2 < n, \quad y_i \sim \begin{cases} F_0, & i = \tau_1 + 1, \dots, \tau_2 \\ F_1, & \text{otherwise} \end{cases}$$

where F_0 and F_1 are two different distribution. We utilize the graph-induced rank proposed by Zhou and Chen (2021)

$$R_{ij} = \sum_{l=1}^k \mathbb{1}((i, j) \in G_l),$$

where $\{G_l\}_{l=1}^k$ is a sequence of similarity graphs with nodes $\{y_i\}_{i=1}^n$ and edges constructed inductively:

$$G_{l+1} = G_l \cup G'_l \text{ with } G'_l = \arg \max_{G' \cap G_l = \emptyset} \sum_{(i, j) \in G'} S_{ij} \text{ s.t. some additional constraints on } G',$$

where $S_{ij} = S(Z_i, Z_j)$ for some similarity measure S , e.g., $S(Z_i, Z_j) = -\|Z_i - Z_j\|$ for Euclidean data, where $\|\cdot\|$ is the Euclidean norm. Many graphs such as k -NNG and the k -minimum spanning tree (k -MST) (Friedman and Rafsky,

1979) satisfy this definition. For example, the constraint on G' for k -NNG is that each node i only points out to one of the other nodes and for k -MST is that G' is a tree connecting all observations. Other choices of graphs are discussed by Zhou and Chen (2021). The graph-induced ranks impose more weights to the edges with higher similarity, thus incorporating more similarity information than the unweighted graph. In the meantime, the robustness property of the ranks makes the weights less sensitive to outliers compared to the direct utilization of similarities. Based on the ranks, we define the two basic quantities

$$U_1(t_1, t_2) = \sum_{i=1}^n \sum_{j=1}^n R_{ij} \mathbb{1}(t_1 < i, j \leq t_2) \text{ and } U_2(t_1, t_2) = \sum_{i=1}^n \sum_{j=1}^n R_{ij} \mathbb{1}(i, j \leq t_1 \text{ or } i, j > t_2).$$

We assume that $\mathbf{R} = (R_{ij})_{i,j=1}^n$ is symmetric, otherwise, it can be replaced by $\frac{1}{2}(\mathbf{R} + \mathbf{R}^\top)$, which does not change the values of $U_1(t_1, t_2)$ and $U_2(t_1, t_2)$. Denote \mathbb{E} , Var and Cov as the expectation, variance and covariance under the permutation null distribution, respectively, which places $1/n!$ probability on each of the $n!$ permutations of the order of the observations. We propose the Mahalanobis-type statistic

$$T_R(t_1, t_2) = \begin{pmatrix} U_1(t_1, t_2) - \mathbb{E}(U_1(t_1, t_2)) \\ U_2(t_1, t_2) - \mathbb{E}(U_2(t_1, t_2)) \end{pmatrix}^\top \Sigma(t_1, t_2)^{-1} \begin{pmatrix} U_1(t_1, t_2) - \mathbb{E}(U_1(t_1, t_2)) \\ U_2(t_1, t_2) - \mathbb{E}(U_2(t_1, t_2)) \end{pmatrix},$$

where $\Sigma(t_1, t_2) = \text{Cov}((U_1(t_1, t_2), U_2(t_1, t_2))^\top)$ and the max-type statistic

$$M_R(t_1, t_2) = \max (Z_w(t_1, t_2), |Z_{\text{diff}}(t_1, t_2)|),$$

where

$$Z_w(t_1, t_2) = \frac{U_w(t_1, t_2) - \mathbb{E}(U_w(t_1, t_2))}{\sqrt{\text{Var}(U_w(t_1, t_2))}} \text{ and } Z_{\text{diff}}(t_1, t_2) = \frac{U_{\text{diff}}(t_1, t_2) - \mathbb{E}(U_{\text{diff}}(t_1, t_2))}{\sqrt{\text{Var}(U_{\text{diff}}(t_1, t_2))}}$$

with $U_{\text{diff}}(t_1, t_2) = U_1(t_1, t_2) - U_2(t_1, t_2)$ and

$$U_w(t_1, t_2) = \frac{n - t_2 + t_1 - 1}{n - 2} U_1(t_1, t_2) + \frac{t_2 - t_1 - 1}{n - 2} U_2(t_1, t_2).$$

The explicit expressions of $\mathbb{E}(U_1(t_1, t_2))$, $\mathbb{E}(U_2(t_1, t_2))$ and $\Sigma(t_1, t_2)$ can be obtained through combinatorial analysis and are presented in Lemma 2.1. The proof is similar to Zhou and Chen (2021), and is thus omitted here. We then define

$$\begin{aligned} R_{i \cdot} &= \sum_{j=1}^n R_{ij}, \quad \bar{R}_{i \cdot} = \frac{R_{i \cdot}}{n-1}, \quad r_0 = \frac{1}{n} \sum_{i=1}^n \bar{R}_{i \cdot}, \\ r_1^2 &= \frac{1}{n} \sum_{i=1}^n \bar{R}_{i \cdot}^2, \quad \text{and} \quad r_d^2 = \frac{1}{n(n-1)} \sum_{i=1}^n \sum_{j=1}^n R_{ij}^2. \end{aligned}$$

Lemma 2.1. *Under the permutation null distribution, we have*

$$\begin{aligned}\mathbb{E}(U_1(t_1, t_2)) &= (t_2 - t_1)(t_2 - t_1 - 1)r_0, \\ \mathbb{E}(U_2(t_1, t_2)) &= (n - t_2 + t_1)(n - t_2 + t_1 - 1)r_0 \\ \text{Var}(U_1(t_1, t_2)) &= A(t_2 - t_1)(r_d^2 - r_0^2) + B(t_2 - t_1)(r_1^2 - r_0^2), \\ \text{Var}(U_2(t_1, t_2)) &= A(n - t_2 + t_1)(r_d^2 - r_0^2) + B(n - t_2 + t_1)(r_1^2 - r_0^2), \\ \text{Cov}(U_1(t_1, t_2), U_2(t_1, t_2)) &= A(t_2 - t_1)((r_d^2 - r_0^2) - 2(n - 1)(r_1^2 - r_0^2)),\end{aligned}$$

where

$$A(t) = \frac{2t(t-1)(n-t)(n-t-1)}{(n-2)(n-3)} \text{ and } B(t) = \frac{4t(n-t)(t-1)(t-2)(n-1)}{(n-2)(n-3)}.$$

Following Theorem 2.3 of Zhou and Chen (2021), we have $T_R(t_1, t_2) = Z_w^2(t_1, t_2) + Z_{\text{diff}}^2(t_1, t_2)$, which builds connection between $T_R(t_1, t_2)$ and $M_R(t_1, t_2)$, and reveals the reason why the two statistics perform well for general distribution changes. The two statistics are widely used by existing literature on two-sample testing and CPD (Chen and Friedman, 2017; Chu and Chen, 2019; Zhou and Chen, 2021). Intuitively, under the alternative hypothesis, it is possible that (i) both $U_1(t_1, t_2)$ and $U_2(t_1, t_2)$ are large under the location alternative and (ii) one of them is large while the other one is small under the scale alternative. For (i), $Z_w(t_1, t_2)$ will be large and for (ii), $|Z_{\text{diff}}(t_1, t_2)|$ will be large. Thus, T_R and M_R are powerful for a wide range of alternatives as they can capture both scenarios.

Let $T_R(t) = T_R(0, t)$ and $M_R(t) = M_R(0, t)$. We consider two sets of scan statistics, one based on T_R 's and the other based on M_R 's. We reject H_0 against H_1 , if the scan statistic

$$\max_{n_0 \leq t \leq n_1} T_R(t)$$

exceeds the critical value for a given significance level. We reject H_0 against H_2 , if the scan statistic

$$\max_{\substack{1 \leq t_1 < t_2 \leq n \\ n_0 \leq t_2 - t_1 \leq n_1}} T_R(t_1, t_2)$$

is large enough. Here n_0 and n_1 are pre-specified integers with the belief that $\tau \in [n_0, n_1]$ for H_1 or $\tau_2 - \tau_1 \in [n_0, n_1]$ for H_2 . A common choice of n_0 and n_1 is $n_0 = [0.05n]$ and $n_1 = n - n_0$, where $[x]$ denotes the integer closest to x . The scan statistics based on M_R 's can be defined similarly. Then the detected change-point is

$$\hat{\tau}_T = \arg \max_{n_0 \leq t \leq n_1} T_R(t) \quad \text{and} \quad \hat{\tau}_M = \arg \max_{n_0 \leq t \leq n_1} M_R(t)$$

and the detected changed interval is

$$[\hat{\tau}_{T1}, \hat{\tau}_{T2}] = \arg \max_{\substack{1 \leq t_1 < t_2 \leq n \\ n_0 \leq t_2 - t_1 \leq n_1}} T_R(t_1, t_2) \quad \text{and} \quad [\hat{\tau}_{M1}, \hat{\tau}_{M2}] = \arg \max_{\substack{1 \leq t_1 < t_2 \leq n \\ n_0 \leq t_2 - t_1 \leq n_1}} M_R(t_1, t_2).$$

3. Asymptotic distribution of the scan statistics

For decision-making, the critical values should be determined. Alternatively, we consider the tail probabilities

$$\mathbb{P}\left(\max_{n_0 \leq t \leq n_1} T_R(t) > b\right), \quad \mathbb{P}\left(\max_{n_0 \leq t \leq n_1} M_R(t) > b\right) \quad (1)$$

for the single change-point alternative and

$$\mathbb{P}\left(\max_{\substack{1 \leq t_1 < t_2 \leq n \\ t_0 \leq t_2 - t_1 \leq l_1}} T_R(t_1, t_2) > b\right), \quad \mathbb{P}\left(\max_{\substack{1 \leq t_1 < t_2 \leq n \\ t_0 \leq t_2 - t_1 \leq l_1}} M_R(t_1, t_2) > b\right) \quad (2)$$

for the changed interval alternative, respectively, where \mathbb{P} denotes the probability under the permutation null distribution. When n is small, we can apply the permutation procedure. However, it is very time-consuming when n is large. Hence, we derive the asymptotic distribution of the scan statistics for the fast approximation of the tail probabilities.

3.1. Asymptotic Null Distributions of the Basic Processes

By the decomposition of $T_R(t)$ and $T_R(t_1, t_2)$ and the definition of $M_R(t)$ and $M_R(t_1, t_2)$, it is sufficient to derive the limiting distributions of

$$\{Z_{\text{diff}}(\lfloor nu \rfloor) : 0 < u < 1\} \text{ and } \{Z_w(\lfloor nu \rfloor) : 0 < u < 1\} \quad (3)$$

for the single change-point alternative where $Z_{\text{diff}}(t) = Z_{\text{diff}}(0, t)$ and $Z_w(t) = Z_w(0, t)$, and

$$\{Z_{\text{diff}}(\lfloor nu \rfloor, \lfloor nv \rfloor) : 0 < u < v < 1\} \text{ and } \{Z_w(\lfloor nu \rfloor, \lfloor nv \rfloor) : 0 < u < v < 1\} \quad (4)$$

for the changed-interval alternative, where $\lfloor x \rfloor$ denotes the largest integer less than or equal to x .

We use the notations $a_n = o(b_n)$ when $\lim_{n \rightarrow \infty} \frac{a_n}{b_n} = 0$ and $a_n \lesssim b_n$ when $\lim_{n \rightarrow \infty} \frac{a_n}{b_n}$ is bounded. Now we list the sufficient conditions to derive the limiting distributions.

Condition 1. $\sum_{i=1}^n \left(\sum_{j=1}^n R_{ij}^2 \right)^2 \lesssim n^3 r_d^4$.

Condition 2. $\sum_{i=1}^n |\bar{R}_{i \cdot} - r_0|^3 = o\left((n(r_1^2 - r_0^2))^{\frac{3}{2}}\right)$.

Condition 3. $\sum_{i=1}^n (\bar{R}_{i \cdot} - r_0)^3 = o(nr_d(r_1^2 - r_0^2))$.

Condition 4. $\left| \sum_{i \neq j \neq k}^n R_{ji} R_{ik} (\bar{R}_{j \cdot} - r_0) (\bar{R}_{k \cdot} - r_0) \right| = o(n^3 r_d^2 (r_1^2 - r_0^2))$.

Condition 5. $\sum_{i=1}^n \sum_{j=1}^n \sum_{k \neq i, j}^n \sum_{l \neq i, j}^n R_{ij} R_{kl} (R_{ik} R_{jl} + R_{il} R_{jk}) = o(n^4 r_d^4)$.

Condition 6. $r_1 = o(r_d)$.

Theorem 3.1. *Under Conditions 1-6, we have*

1. $\{Z_{\text{diff}}(\lfloor nu \rfloor) : 0 < u < 1\}$ and $\{Z_w(\lfloor nu \rfloor) : 0 < u < 1\}$ converge to independent Gaussian processes in finite dimensional distributions, which we denote as $\{Z_{\text{diff}}^*(u) : 0 < u < 1\}$ and $\{Z_w^*(u) : 0 < u < 1\}$, respectively.
2. $\{Z_{\text{diff}}(\lfloor nu \rfloor, \lfloor nv \rfloor) : 0 < u < v < 1\}$ and $\{Z_w(\lfloor nu \rfloor, \lfloor nv \rfloor) : 0 < u < v < 1\}$ converge to independent two-dimension Gaussian random fields in finite dimensional distributions, which we denote as $\{Z_{\text{diff}}^*(u, v) : 0 < u < v < 1\}$ and $\{Z_w^*(u, v) : 0 < u < v < 1\}$, respectively.

Remark 1. The Conditions 1-6 are the same as Zhou and Chen (2021) and are discussed in detail there. The conditions are mild and allow the non-zero entries to be the order of $n^{1+\alpha}$ for some $0 < \alpha < 1$. The result is inspiring as we do not need extra conditions when we extend the statistics from two-sample testing to the scan statistics for the CPD.

The proof of Theorem 3.1 is deferred to Supplement S1. Let $\rho_w^*(u, v) = \mathbf{Cov}(Z_w^*(u), Z_w^*(v))$ and $\rho_{\text{diff}}^*(u, v) = \mathbf{Cov}(Z_{\text{diff}}^*(u), Z_{\text{diff}}^*(v))$. We give the explicit formula of $\rho_w^*(u, v)$ and $\rho_{\text{diff}}^*(u, v)$ in Theorem 3.2, whose proof is in Supplement S2.

Theorem 3.2. *The exact expressions for $\rho_{\text{diff}}^*(u, v)$ and $\rho_w^*(u, v)$ are*

$$\rho_w^*(u, v) = \frac{(u \wedge v)(1 - (u \vee v))}{(u \vee v)(1 - (u \wedge v))},$$

$$\rho_{\text{diff}}^*(u, v) = \frac{(u \wedge v)(1 - (u \vee v))}{\sqrt{(u \wedge v)(1 - (u \wedge v))(u \vee v)(1 - (u \vee v))}},$$

where $u \wedge v = \min(u, v)$ and $u \vee v = \max(u, v)$.

Theorems 3.1 and 3.2 together show that the limiting distributions of (3) and (4) are independent of \mathbf{R} , thus asymptotically distribution-free. As a result, the proposed statistics based on (3) and (4) are also asymptotically distribution-free.

3.2. Tail Probabilities

Based on Theorems 3.1 and 3.2, following the routine of Chu and Chen (2019), we can approximate (1) by

$$\mathbb{P}\left(\max_{n_0 \leq t \leq n_1} T_R(t) > b\right) \approx \frac{be^{-b/2}}{2\pi} \int_0^{2\pi} \int_{\frac{n_0}{n}}^{\frac{n_1}{n}} u(x, \omega) \nu(\sqrt{2bu(x, \omega)/n}) dx d\omega, \quad (5)$$

$$\begin{aligned} \mathbb{P}\left(\max_{\substack{1 \leq t_1 < t_2 \leq n \\ t_0 \leq t_2 - t_1 \leq t_1}} T_R(t_1, t_2) > b\right) \\ \approx \frac{b^2 e^{-b/2}}{2\pi} \int_0^{2\pi} \int_{\frac{t_0}{n}}^{\frac{t_1}{n}} u(x, \omega) \nu(\sqrt{2bu(x, \omega)/n})^2 (1 - x) dx d\omega, \end{aligned} \quad (6)$$

where $u(x, \omega) = h_w(n, x) \sin^2(\omega) + h_{\text{diff}}(x) \cos^2(\omega)$ with

$$h_w(n, x) = \frac{(n-1)(2nx^2 - 2nx + 1)}{2x(1-x)(nx-1)(nx-n+1)} \quad \text{and} \quad h_{\text{diff}}(n, x) = \frac{1}{2x(1-x)}.$$

Here $v(x)$ is approximated (Siegmund and Yakir, 2007) as

$$v(x) \approx \frac{(2/x)(\Phi(x/2) - 0.5)}{(x/2)\Phi(x/2) + \phi(x/2)},$$

where $\Phi(\cdot)$ and $\phi(\cdot)$ denote the standard normal cumulative density function and standard normal density function, respectively. We also have

$$\mathbb{P}\left(\max_{n_0 \leq t \leq n_1} M_R(t) > b\right) \approx 1 - \mathbb{P}\left(\max_{n_0 \leq t \leq n_1} Z_w(t) < b\right) \mathbb{P}\left(\max_{n_0 \leq t \leq n_1} |Z_{\text{diff}}(t)| < b\right), \quad (7)$$

$$\begin{aligned} & \mathbb{P}\left(\max_{\substack{1 \leq t_1 < t_2 \leq n \\ t_0 \leq t_2 - t_1 \leq l_1}} M_R(t_1, t_2) > b > b\right) \\ & \approx 1 - \mathbb{P}\left(\max_{l_0 \leq t_2 - t_1 \leq l_1} Z_w(t_1, t_2) < b\right) \mathbb{P}\left(\max_{l_0 \leq t_2 - t_1 \leq l_1} |Z_{\text{diff}}(t_1, t_2)| < b\right), \end{aligned} \quad (8)$$

where

$$\mathbb{P}\left(\max_{n_0 \leq t \leq n_1} Z_w(t) > b\right) \approx b\phi(b) \int_{\frac{n_0}{n}}^{\frac{n_1}{n}} h_w(n, x)\nu(b\sqrt{2h_w(n, x)/n})dx, \quad (9)$$

$$\begin{aligned} & \mathbb{P}\left(\max_{l_0 \leq t_2 - t_1 \leq l_1} Z_w(t_1, t_2) > b\right) \\ & \approx b^3\phi(b) \int_{\frac{l_0}{n}}^{\frac{l_1}{n}} \left(h_w(n, x)\nu(b\sqrt{2h_w(n, x)/n})\right)^2 (1-x)dx, \end{aligned} \quad (10)$$

$$\mathbb{P}\left(\max_{n_0 \leq t \leq n_1} Z_{\text{diff}}(t) > b\right) \approx b\phi(b) \int_{\frac{n_0}{n}}^{\frac{n_1}{n}} h_{\text{diff}}(n, x)\nu(b\sqrt{2h_{\text{diff}}(n, x)/n})dx, \quad (11)$$

$$\begin{aligned} & \mathbb{P}\left(\max_{l_0 \leq t_2 - t_1 \leq l_1} Z_{\text{diff}}(t_1, t_2) > b\right) \\ & \approx b^3\phi(b) \int_{\frac{l_0}{n}}^{\frac{l_1}{n}} \left(h_{\text{diff}}(n, x)\nu(b\sqrt{2h_{\text{diff}}(n, x)/n})\right)^2 (1-x)dx. \end{aligned} \quad (12)$$

3.3. Skewness Correction

As observed by Chen and Zhang (2015); Chu and Chen (2019), the analytical approximations can be improved by skewness correction when n_0 and $n - n_1$ decrease. To be specific, instead of using (9)-(12) to approximate (7) and (8),

we use

$$\mathbb{P}\left(\max_{n_0 \leq t \leq n_1} Z_w(t) > b\right) \approx b\phi(b) \int_{\frac{n_0}{n}}^{\frac{n_1}{n}} K_w(nx)h_w(n, x)\nu(b\sqrt{2h_w(n, x)/n})dx, \quad (13)$$

$$\begin{aligned} \mathbb{P}\left(\max_{l_0 \leq t_2 - t_1 \leq l_1} Z_w(t_1, t_2) > b\right) \\ \approx b^3\phi(b) \int_{\frac{l_0}{n}}^{\frac{l_1}{n}} K_w(nx)\left(h_w(n, x)\nu(b\sqrt{2h_w(n, x)/n})\right)^2(1-x)dx, \end{aligned} \quad (14)$$

$$\mathbb{P}\left(\max_{n_0 \leq t \leq n_1} Z_{\text{diff}}(t) > b\right) \approx b\phi(b) \int_{\frac{n_0}{n}}^{\frac{n_1}{n}} K_{\text{diff}}(nx)h_{\text{diff}}(n, x)\nu(b\sqrt{2h_{\text{diff}}(n, x)/n})dx, \quad (15)$$

$$\begin{aligned} \mathbb{P}\left(\max_{l_0 \leq t_2 - t_1 \leq l_1} Z_{\text{diff}}(t_1, t_2) > b\right) \\ \approx b^3\phi(b) \int_{\frac{l_0}{n}}^{\frac{l_1}{n}} K_{\text{diff}}(nx)\left(h_{\text{diff}}(n, x)\nu(b\sqrt{2h_{\text{diff}}(n, x)/n})\right)^2(1-x)dx, \end{aligned} \quad (16)$$

where for $j = w, \text{diff}$,

$$K_j(t) = \frac{\exp\left(\frac{1}{2}(b - \hat{\theta}_{b,j}(t))^2 + \frac{1}{6}\gamma_j(t)\hat{\theta}_{b,j}(t)^3\right)}{\sqrt{1 + \gamma_j(t)\hat{\theta}_{b,j}(t)}}$$

with $\hat{\theta}_{b,j}(t) = \frac{-1+\sqrt{1+2\gamma_j(t)b}}{\gamma_j(t)}$ and $\gamma_j(t) = \mathbb{E}(Z_j^3(t))$. The only unknown quantities in the above expressions are $\gamma_w(t)$ and $\gamma_{\text{diff}}(t)$, whose exact analytic expressions are quite long and provided in Supplement S3.

3.4. Assessment of the finite sample approximations

Here we assess the performance of the asymptotic approximations with finite samples. For a constant ρ , we define the first-order auto-regressive correlation matrix $\Sigma(\rho) = (\rho^{|i-j|})_{i,j=1}^d \in \mathbb{R}^{d \times d}$. We consider three distributions for three different dimensions $d = 20, 100$ and 1000 with $n = 1000$:

- i. the multivariate Gaussian distribution $y_i \sim N_d(\mathbf{0}_d, \Sigma(0.6))$;
- ii. the multivariate t_5 distribution $y_i \sim t_5(\mathbf{0}_d, \Sigma(0.5))$;
- iii. the multivariate log-normal distribution $y_i \sim \exp(N_d(\mathbf{0}_d, \Sigma(0.4)))$.

We compare the critical values obtained from the analytical formulas to those from 10,000 random permutations, which can be viewed as a good approximation to the true critical values. Here, we focus on the graph-induced rank in k -NNG. We denote the $T_R(t)$ and $M_R(t)$ scan statistics on the graph-induced rank in k -NNG by T_g -NN and M_g -NN. In Table 1, we show the asymptotic critical values obtained from (5) labeled by (A1) at $\alpha = 0.05$ significance level

TABLE 1

Critical values for the single change-point scan statistic T_g -NN at $\alpha = 0.05$ significance level with $n = 1000$ and $d = 20, 100, 100$ under setting (i), (ii) and (iii). The k -NN graph for various k are considered. Here $k_1 = [n^{0.5}]$, $k_1 = [n^{0.65}]$ and $k_3 = [n^{0.8}]$.

		$n_0 = 100$				$n_0 = 75$				$n_0 = 50$				$n_0 = 25$					
		A1			13.10			13.38			13.70			14.11					
		Critical values based on 10,000 permutations for T_g -NN.																	
$\frac{d}{k}$	i	$n_0 = 100$			$n_0 = 75$			$n_0 = 50$			$n_0 = 25$								
		20	100	1000	20	100	1000	20	100	1000	20	100	1000	20	100	1000	20	100	1000
5		13.09	13.14	13.73	13.49	13.65	14.41	13.98	14.57	15.65	15.26	15.99	18.88						
10		12.97	12.98	13.16	13.45	13.59	14.11	13.79	14.41	15.22	14.98	15.50	17.27						
k_1		13.45	13.17	13.30	14.13	13.68	13.56	14.51	14.16	14.41	15.28	15.06	15.76						
k_2		14.20	13.09	13.02	14.38	14.05	13.54	15.37	14.07	13.99	16.16	15.07	14.73						
k_3		16.05	13.92	12.98	16.53	14.24	13.29	17.28	14.89	13.64	18.16	15.53	14.29						
ii		$n_0 = 100$			$n_0 = 75$			$n_0 = 50$			$n_0 = 25$								
$\frac{d}{k}$	ii	20	100	1000	20	100	1000	20	100	1000	20	100	1000	20	100	1000	20	100	1000
5		13.06	13.75	15.61	13.51	14.05	16.96	13.83	15.30	19.87	15.45	18.19	25.99						
10		13.14	13.57	14.59	13.62	14.39	16.02	14.29	15.02	17.77	15.13	17.53	22.54						
k_1		13.81	13.83	14.13	13.88	14.28	14.46	14.80	15.32	15.68	15.80	16.78	17.56						
k_2		15.02	14.36	13.43	15.57	14.68	13.96	16.27	15.05	14.43	17.36	16.31	15.86						
k_3		17.47	14.50	13.08	17.84	15.00	13.43	19.45	15.50	14.15	19.85	16.29	14.64						
iii		$n_0 = 100$			$n_0 = 75$			$n_0 = 50$			$n_0 = 25$								
$\frac{d}{k}$	iii	20	100	1000	20	100	1000	20	100	1000	20	100	1000	20	100	1000	20	100	1000
5		12.94	13.46	15.19	13.58	13.87	16.10	13.99	14.88	18.93	15.25	16.71	24.52						
10		13.27	13.57	14.10	13.64	14.34	15.24	13.79	15.11	17.43	15.09	16.59	20.35						
k_1		14.04	13.98	13.35	14.36	14.53	14.06	15.06	15.40	15.28	16.09	16.80	17.08						
k_2		15.47	14.59	13.19	16.46	15.06	13.84	16.85	15.45	14.24	18.16	16.82	15.48						
k_3		17.82	14.36	13.24	18.29	14.66	13.67	19.54	15.63	13.80	20.38	16.62	14.69						

for T_g -NN with various k 's. We notice that when n_0 is large enough ($n_0 \geq 50$), the analytic critical values approximations are reasonably well for a wide range of k ($k \leq [n^{0.65}]$). When n_0 is small, the critical values are preciser for less dense graphs and low dimensions. Table 2 presents the asymptotic critical values obtained from (7) with (9) (labeled A1) and the skewness corrected critical values obtained from (7) with (13) (labeled A2) at $\alpha = 0.05$ significance level for M_g -NN with various k 's. The critical values obtained from 10,000 permutations are labeled by 'Per'. We see that the skewness corrected critical values are more accurate than the critical values without skewness correction in most of the cases.

TABLE 2

Critical values for the single change-point scan statistic M_g -NN based on at $\alpha = 0.05$ significance level with $n = 1000$ and $d = 20, 100, 1000$ under setting (i), (ii) and (iii). The k -NN graph for various k are considered. Here $k_1 = [n^{0.5}]$, $k_1 = [n^{0.65}]$ and $k_3 = [n^{0.8}]$.

	$n_0 = 100$			$n_0 = 75$			$n_0 = 50$			$n_0 = 25$		
	A1			3.23			3.27			3.32		

Critical values based on 10,000 permutations and skewness correction for M_g -NN.													
i	$n_0 = 100$			$n_0 = 75$			$n_0 = 50$			$n_0 = 25$			
	k	d	20	100	1000	20	100	1000	20	100	1000	20	100
5 (A2)	3.29	3.28	3.26	3.35	3.34	3.32	3.42	3.43	3.38	3.55	3.58	3.50	
5 (Per)	3.26	3.28	3.32	3.37	3.37	3.42	3.43	3.49	3.59	3.63	3.69	3.99	
10 (A2)	3.30	3.28	3.26	3.35	3.34	3.31	3.42	3.42	3.37	3.54	3.55	3.47	
10 (Per)	3.29	3.28	3.28	3.35	3.33	3.40	3.45	3.47	3.55	3.61	3.63	3.82	
k_1 (A2)	3.34	3.30	3.28	3.39	3.36	3.34	3.45	3.42	3.42	3.55	3.53	3.54	
k_1 (Per)	3.37	3.29	3.27	3.45	3.38	3.34	3.51	3.45	3.45	3.63	3.59	3.65	
k_2 (A2)	3.45	3.34	3.28	3.46	3.39	3.33	3.52	3.45	3.39	3.61	3.54	3.49	
k_2 (P)	3.49	3.35	3.25	3.50	3.45	3.34	3.62	3.45	3.43	3.71	3.59	3.50	
k_3 (A2)	3.58	3.44	3.33	3.64	3.46	3.35	3.66	3.52	3.40	3.74	3.60	3.48	
k_3 (Per)	3.70	3.50	3.31	3.76	3.52	3.36	3.86	3.60	3.38	3.96	3.70	3.48	
ii	$n_0 = 100$			$n_0 = 75$			$n_0 = 50$			$n_0 = 25$			
k	d	20	100	1000	20	100	1000	20	100	1000	20	100	1000
5 (A2)	3.29	3.30	3.25	3.34	3.37	3.29	3.42	3.43	3.35	3.54	3.49	3.44	
5 (Per)	3.31	3.32	3.42	3.34	3.36	3.59	3.42	3.53	3.83	3.64	3.90	4.33	
10 (A2)	3.30	3.31	3.25	3.36	3.37	3.29	3.42	3.46	3.35	3.54	3.60	3.42	
10 (Per)	3.31	3.31	3.37	3.35	3.40	3.49	3.47	3.49	3.68	3.58	3.78	4.08	
k_1 (A2)	3.35	3.32	3.28	3.40	3.38	3.35	3.46	3.45	3.42	3.56	3.57	3.55	
k_1 (Per)	3.39	3.33	3.31	3.42	3.38	3.35	3.54	3.54	3.51	3.65	3.70	3.74	
k_2 (A2)	3.46	3.36	3.28	3.48	3.41	3.33	3.54	3.47	3.39	3.63	3.56	3.48	
k_2 (Per)	3.44	3.40	3.29	3.61	3.44	3.36	3.63	3.49	3.40	3.74	3.64	3.56	
k_3 (A2)	3.59	3.41	3.30	3.64	3.46	3.34	3.66	3.52	3.40	3.74	3.60	3.47	
k_3 (Per)	3.74	3.43	3.28	3.77	3.49	3.31	3.84	3.57	3.41	3.98	3.68	3.48	
iii	$n_0 = 100$			$n_0 = 75$			$n_0 = 50$			$n_0 = 25$			
k	d	20	100	1000	20	100	1000	20	100	1000	20	100	1000
5 (A2)	3.33	3.30	3.26	3.38	3.36	3.31	3.42	3.45	3.37	3.55	3.60	3.46	
5 (Per)	3.31	3.31	3.44	3.35	3.36	3.56	3.46	3.51	3.78	3.64	3.74	4.32	
10 (A2)	3.35	3.31	3.26	3.40	3.37	3.30	3.44	3.45	3.36	3.55	3.59	3.45	
10 (Per)	3.33	3.31	3.37	3.39	3.40	3.50	3.44	3.50	3.75	3.60	3.68	4.02	
k_1 (A2)	3.37	3.33	3.30	3.42	3.39	3.34	3.49	3.46	3.36	3.58	3.58	3.44	
k_1 (Per)	3.38	3.32	3.29	3.43	3.38	3.40	3.56	3.52	3.53	3.66	3.66	3.79	
k_2 (A2)	3.49	3.36	3.28	3.50	3.41	3.33	3.57	3.48	3.39	3.65	3.57	3.49	
k_2 (Per)	3.50	3.40	3.29	3.58	3.42	3.37	3.62	3.49	3.42	3.77	3.65	3.57	
k_3 (A2)	3.60	3.39	3.29	3.65	3.44	3.34	3.67	3.50	3.39	3.75	3.58	3.47	
k_3 (Per)	3.67	3.40	3.30	3.74	3.42	3.37	3.88	3.53	3.37	3.98	3.66	3.50	

3.5. Consistency

We here examine the consistency of T_R and M_R for the k -NNG and k -MST. At first, we define the limits

$$T(\delta_1, \delta_2) = \lim_{n \rightarrow \infty} \frac{T_R([\delta_1 n], [\delta_2 n])}{n} \text{ and } T(\delta) = T(0, \delta) \text{ and}$$

$$M(\delta_1, \delta_2) = \lim_{n \rightarrow \infty} \frac{M_R([\delta_1 n], [\delta_2 n])}{\sqrt{n}} \text{ and } M(\delta) = M(0, \delta).$$

Theorem 3.3. *Consider two continuous multivariate distributions F_0 and F_1 which are different in a positive measure, and the graph-induced rank is used with the k -MST or k -NNG based on the Euclidean distance, where $k = O(1)$.*

- For the change-point alternative H_1 : let $\omega = \lim_{n \rightarrow \infty} \tau/n \in (0, 1)$, $\hat{\omega}_T = \hat{\tau}_T/n$ and $\hat{\omega}_M = \hat{\tau}_M/n$. Assume that

$$\sup_{\delta \in (0, 1)} \left| \frac{T_R([\delta n])}{n} - T(\delta) \right| \xrightarrow{P} 0 \text{ and } \sup_{\delta \in (0, 1)} \left| \frac{M_R([\delta n])}{\sqrt{n}} - M(\delta) \right| \xrightarrow{P} 0, \quad (17)$$

Then the scan statistics of $T_R(t)$ and $M_R(t)$ are consistent in that they will reject H_0 against H_1 with probability goes to one for any significance level $0 < \alpha < 1$ and

$$\mathbb{P}(|\hat{\omega}_T - \omega| > \epsilon) \rightarrow 0 \text{ and } \mathbb{P}(|\hat{\omega}_M - \omega| > \epsilon) \rightarrow 0 \text{ for any } \epsilon > 0.$$

- For the changed interval alternative H_2 : let $\omega_i = \lim_{n \rightarrow \infty} \tau_i/n \in (0, 1)$, $\hat{\omega}_{Ti} = \hat{\tau}_{Ti}/n$ and $\hat{\omega}_{Mi} = \hat{\tau}_{Mi}/n$ for $i = 1, 2$. Assume that $\omega_2 - \omega_1 > 0$ and

$$\begin{aligned} & \sup_{0 < \delta_1 < \delta_2 < 1} \left| \frac{T_R([\delta_1 n], [\delta_2 n])}{n} - T(\delta_1, \delta_2) \right| \xrightarrow{P} 0 \text{ and} \\ & \sup_{0 < \delta_1 < \delta_2 < 1} \left| \frac{M_R([\delta_1 n], [\delta_2 n])}{\sqrt{n}} - M(\delta_1, \delta_2) \right| \xrightarrow{P} 0, \end{aligned} \quad (18)$$

then the scan statistics of $T_R(t_1, t_2)$ and $M_R(t_1, t_2)$ are consistent in that they will reject H_0 against H_2 with probability goes to one for any significance level $0 < \alpha < 1$ and

$$\mathbb{P}(\cup_{i=1}^2 \{|\hat{\omega}_{Ti} - \omega_i| > \epsilon\}) \rightarrow 0 \text{ and } \mathbb{P}(\cup_{i=1}^2 \{|\hat{\omega}_{Mi} - \omega_i| > \epsilon\}) \rightarrow 0 \text{ for any } \epsilon > 0.$$

The proof of this theorem is in Supplement S4. Although Assumptions (17) and (18) are reasonable, their verification of is difficult and is left for future work. Here we check them numerically through Monte Carlo simulations. Specifically, we consider the following combinations of (F_0, F_1) with $\omega = 0.5$ and $d = 500$:

- (i) the multivariate Gaussian distribution $(N_d(\mathbf{0}_d, \mathbf{I}_d), N_d(0.1\mathbf{1}_d, \mathbf{I}_d))$;
- (ii) the multivariate t_3 distribution $(t_3(\mathbf{0}_d, \mathbf{I}_d), t_3(0.1\mathbf{1}_d, 1.02^2\mathbf{I}_d))$;

- (iii) the multivariate Cauchy distribution $(\text{Cauchy}_d(\mathbf{0}_d, \mathbf{I}_d), \text{Cauchy}_d(2\mathbf{1}_d, \mathbf{I}_d))$.

We generate 10 independent sequences for each setting and the plots of $T_R([\delta n])/n$ and $M_R([\delta n])/\sqrt{n}$ against δ for various values of n are presented Figures 1 and 2. These plots verify the assumption that $T_R([\delta n])/n$ and $M_R([\delta n])/\sqrt{n}$ converge when $n \rightarrow \infty$.

4. Simulation studies

4.1. The Choice of k

The choice of graphs remains an open question for CPD based on similarity graphs (Friedman and Rafsky, 1979; Zhang and Chen, 2020; Chen and Friedman, 2017; Chen, Chen and Su, 2018). We adapt the method in Zhang and Chen (2021) and Zhou and Chen (2021) after Zhu and Chen (2021) observed the improvement of power by using denser graphs. Specifically, they consider the power of their method for $k = [n^\lambda]$ when varying λ from 0 to 1. Zhu and Chen (2021) suggested to use $k = [n^{0.5}]$ for GET with the k -MST while Zhou and Chen (2021) recommended $k = [n^{0.65}]$ for the Mahalanobis-type statistic with graph-based rank on the k -NNG. We follow the same way to choose k for T_g -NN and M_g -NN. Specifically, we generate independent sequences from three difference distribution pairs of (F_0, F_1) :

- (i) the multivariate Gaussian distribution $(N_d(\mathbf{0}_d, \mathbf{I}_d), N_d(\frac{30}{\sqrt{Nd}}\mathbf{1}_d, \mathbf{I}_d))$;
- (ii) the multivariate t_3 distribution $(t_3(\mathbf{0}_d, \mathbf{I}_d), t_3(\frac{30}{\sqrt{Nd}}\mathbf{1}_d, (1 + \frac{30}{\sqrt{Nd}})^2\mathbf{I}_d))$;
- (iii) the multivariate Cauchy distribution $(\text{Cauchy}_d(\mathbf{0}_d, \mathbf{I}_d), \text{Cauchy}_d(\frac{30}{\sqrt{N}}\mathbf{1}_d, \mathbf{I}_d))$.

The parameters are set to make these tests have moderate power. The change-point $\tau = n/2$, the dimension $d = 500$ and $n = 50, 100, 200$. We set $n_0 = \lceil 0.05n \rceil$ and $n_1 = n - n_0$, which will also be our choice by default in the latter experiments. For comparison, we also show the result of GET and MET using k -MST. The detection power is defined as the ratio of successful detection where the p -value is smaller than 0.05 and the detected change-point is in the interval $[\tau - 0.05n, \tau + 0.05n]$. For fairness, the p -values are obtained through 1,000 permutations for all methods.

Figure 3 shows the power of these tests for $k = [n^\lambda]$. First, we see that T_g -NN and M_g -NN have similar performance. The power of these tests first increase quickly when k or λ increase. If k continues to increase, the power of GET and MET decreases dramatically, but the power of T_g -NN and M_g -NN seems more robust. The overall performances of T_g -NN and M_g -NN are the best, with a significant improvement of the power over heavy-tailed settings (the multivariate t_3 and Cauchy distributions) and the robustness over a wide range choice of k . Finally, we choose $\lambda = 0.65$ for T_g -NN and M_g -NN, and $\lambda = 0.5$ for GET and MET in the following analysis, which is reasonable for these methods to achieve adequate power and coincides with previous choices (Zhang and Chen, 2021; Zhou and Chen, 2021).

4.2. Performance comparison

We compare the proposed method to GET and MET on k -MST using the R package *gSeg* (Chu and Chen, 2019) with $k = \lceil \sqrt{n} \rceil$, the method using Bayesian-type statistic based on the shortest Hamiltonian path (Shi, Wu and Rao, 2017) (SWR), the method based on Fréchet means and variances (Dubey and Müller, 2020) (DM). We also compare with three interpoint distance-based methods, the widely used distance-based method E-Divisive (ED) (Matteson and James, 2014) implemented in the R package *ecp*, and the other two methods proposed recently by Li (2020) and Nie and Nicolae (2021). Li (2020) proposed four statistics and we compare the statistic C_{2N} that had the satisfactory performance in most of their simulation settings. Nie and Nicolae (2021) proposed three test statistics, which preform well for location change, scale change and general change, respectively. Here we compare with their statistic S_3 , which they concluded to have relative robust performance across various alternative. For fairness, the p -values of these methods are decided by 1,000 permutations.

We set $n = 200$ and the change-point $\tau = \lceil \frac{n}{3} \rceil$ and consider the dimension of the distributions $d = 200, 500, 1000$. Before the change-point, $y_i \sim F_0$ and after the change-point, $y_i \sim F_1$. We consider both the empirical power and the detection accuracy. The empirical power is the ratio of the successfully detection defined as p -value no larger than the significance level $\alpha = 0.05$ out of 1,000 trails. The detection accuracy is provided in parentheses, which is the ratio of trails that the detected change-point is within 10 from the the true change-point and the p -value no larger than α . We consider various settings which cover the light-tailed, heavy-tailed, skewed, mixture distributions and the distribution with outliers for location, scale, and mixed alternatives. Specifically, we consider the six settings for F_i , $i = 0, 1$:

- (I) the multivariate Gaussian distribution $N_d(\boldsymbol{\mu}_i, \boldsymbol{\Sigma}_i)$;
- (II) the multivariate t_5 distribution $t_5(\boldsymbol{\mu}_i, \boldsymbol{\Sigma}_i)$;
- (III) the multivariate Cauchy distribution $\text{Cauchy}(\boldsymbol{\mu}_i, \boldsymbol{\Sigma}_i)$;
- (IV) the multivariate χ_5^2 distribution $\chi_5^2(\boldsymbol{\mu}_i, \boldsymbol{\Sigma}_i)$ (generated as $\boldsymbol{\Sigma}_i^{\frac{1}{2}}(X - 5\mathbf{1}_d + \boldsymbol{\mu}_i)$ where the d components of X are i.i.d. χ_5^2);
- (V) the Gaussian mixture distribution $WN_d(\boldsymbol{\mu}_i, \boldsymbol{\Sigma}_i) + (1 - W)N_d(-\boldsymbol{\mu}_i, \boldsymbol{\Sigma}_i)$ with $W \sim \text{Bernoulli}(0.5)$;
- (VI) the multivariate normal distribution with t_7 outliers $WN_d(\boldsymbol{\mu}_i, \boldsymbol{\Sigma}_i) + (1 - W)t_7(\boldsymbol{\mu}_i, \boldsymbol{\Sigma}_i)$ with $W \sim \text{Bernoulli}(0.9)$.

We set $\boldsymbol{\mu}_0 = \mathbf{0}_d$ for F_0 and $\boldsymbol{\mu}_1 = \delta\mathbf{1}_d$ for F_1 , where δ is different for different settings. For each setting, we consider five different alternatives:

- (a) location ($\delta \neq 0$ and $\boldsymbol{\Sigma}_1 = \boldsymbol{\Sigma}_0$);
- (b) simple scale ($\delta = 0$ and $\boldsymbol{\Sigma}_1 = (1 + \sigma)^2\boldsymbol{\Sigma}_0$);
- (c) complex scale ($\delta = 0$ and $\boldsymbol{\Sigma}_1 \neq \boldsymbol{\Sigma}_0$);
- (d) location and simple scale mixed ($\delta \neq 0$ and $\boldsymbol{\Sigma}_1 = (1 + \sigma)^2\boldsymbol{\Sigma}_0$);
- (e) location and complex scale mixed ($\delta \neq 0$ and $\boldsymbol{\Sigma}_1 \neq \boldsymbol{\Sigma}_0$).

The choice of δ , σ and $\boldsymbol{\Sigma}_i$, $i = 1, 2$ are specified differently for the settings and

TABLE 3
The specific changes for different settings and alternatives.

Setting	H_0 Σ_0	Alternative					
		(a) δ	(b) σ	(c) Σ_1	(d) δ	(d) σ	(e) δ
(I)	$\Sigma(0.6)$	$\frac{2 \log d}{5\sqrt{d}}$	$\sqrt{\frac{\log d}{16d}}$	$\Sigma(0.16)$	$\frac{\log d}{10\sqrt{d}}$	$\sqrt{\frac{\log d}{16d}}$	$\sqrt{\frac{\log d}{4d}}$
(II)	$\Sigma(0.6)$	$\frac{5 \log d}{4\sqrt{d}}$	$\frac{3 \log d}{10\sqrt{d}}$	$0.6\Sigma(0.1)$	$\frac{\log d}{3\sqrt{d}}$	$\sqrt{\frac{3 \log d}{10\sqrt{d}}}$	$\frac{\log d}{2\sqrt{d}}$
(III)	$\Sigma(0.4)$	$\frac{11 \log d}{20\sqrt{d}}$	$\frac{6 \log d}{5d^{2/5}}$	$\Sigma(0.85)$	$\frac{6 \log d}{25d^{2/5}}$	$\sqrt{\frac{\log d}{25d}}$	$\frac{6 \log d}{25d^{2/5}}$
(IV)	\mathbf{A}_0	$\frac{5 \log d}{2\sqrt{d}}$	$\frac{9}{10\sqrt{d}}$	\mathbf{A}_1	$\sqrt{\frac{49 \log d}{16d}}$	$\frac{3}{4\sqrt{d}}$	$\sqrt{\frac{49 \log d}{16d}}$
(V)	\mathbf{I}_d	$\frac{3}{5\log d}$	$\sqrt{\frac{\log d}{25d}}$	$\Sigma(0.55)$	$\frac{3}{10\log d}$	$\sqrt{\frac{\log d}{25d}}$	$\frac{3}{10\log d}$
(VI)	$\Sigma(0.5)$	$\frac{7 \log d}{20\sqrt{d}}$	$\frac{\log d}{5\sqrt{d}}$	$\Sigma(0.1)$	$\frac{\log d}{5\sqrt{d}}$	$\frac{\log d}{5\sqrt{d}}$	$\Sigma(0.15)$

alternatives, summarized in Table 3, where the changes in signal are set to make these tests have moderate power. Here for Setting IV, the covariance matrices $\mathbf{A}_i = \mathbf{V}\mathbf{B}_i\mathbf{V}$, for $i = 0, 1, 2$, where \mathbf{V} is a diagonal matrix with the diagonal elements sampled independently from $U(1, 3)$, $\mathbf{B}_i = \text{diag}(\mathbf{B}_{i1}, \dots, \mathbf{B}_{i\frac{d}{10}})$ is a block-diagonal correlation matrix. Each diagonal block \mathbf{B}_{ij} is a 10×10 matrix with diagonal entries being 1 and off-diagonal entries equal to $\rho_{ij} \sim U(a_j, b_j)$ independently. We set $a_0 = 0, b_0 = 0.5, a_1 = 0.3, b_1 = 0.8$ and $a_3 = 0.2, b_3 = 0.7$. We present the result of Settings I-III in Table 4, and the result of Settings IV-VI in Table 5.

From Table 4, we see that for the multivariate normal distribution, under the location alternative (a), ED and C_{2N} perform the best, followed immediately by T_g -NN and M_g -NN. S_3 performs the best for the simple scale alternative (b), followed immediately by C_{2N} , T_g -NN and M_g -NN. For the complex scale alternative (c), T_g -NN and M_g -NN outperform other methods, and SWR also performs well, while other methods have low power. For the location and simple scale mixed alternative (d), S_3 performs the best, C_{2N} , T_g -NN, M_g -NN, GET and MET also have satisfactory performance. For the location and complex scale mixed alternative (e), T_g -NN and M_g -NN perform the best again. The overall performances of T_g -NN and M_g -NN are the best in the multivariate normal setting I.

Besides, for the multivariate t_5 and Cauchy distributions, T_g -NN and M_g -NN show the highest power under the alternatives (a), (b), (d), and (e). SWR performs the best for the complex scale alternative (c), followed immediately by T_g -NN and M_g -NN. GET and MET also have moderate power. On the contrary, DM, ED, C_{2N} and S_3 fail for most of the alternatives under the multivariate t_5 and Cauchy distributions with the power near the significance level. It shows that T_g -NN and M_g -NN are robust to heavy-tailed distributions, while other methods such as C_{2N} and S_3 can not work well as they require the existence of the second moment.

From Table 5, we see that ED and C_{2N} perform the best for the location alternative (a) under the multivariate χ_5^2 distribution, while T_g -NN and M_g -NN perform the second best. In addition, under the same distribution, T_g -NN

TABLE 4

The power of the tests under Settings I-III with the location alternative (a), the simple scale alternative (b), the complex scale alternative (c), the location and simple scale mixed alternative (d) and the location and complex scale mixed alternative (e) where the nominal significance level $\alpha = 0.05$, for $n = 200$, $\tau = [\frac{n}{3}]$ and $d = 200, 500, 1000$.

	Setting I (Gaussian)			Setting II (t_5)			Setting III (Cauchy)		
	200	500	1000	200	500	1000	200	500	1000
Location Alternative (a)									
T _g -NN	73(55)	63(46)	55(37)	86(67)	74 (56)	60(41)	96(85)	81(69)	55(42)
M _g -NN	76(58)	67(49)	59(40)	89(71)	79(59)	67(49)	99(88)	91(78)	72(55)
GET	63(46)	52(36)	40(25)	68(48)	41(26)	20(12)	85(72)	54(40)	28(17)
MET	68(50)	58(39)	46(30)	75(52)	50(32)	31(18)	90(75)	67(50)	44(26)
SWR	21(8)	18(6)	16(4)	19(6)	19(6)	15(4)	44(23)	40(18)	32(15)
DM	7(0)	6(0)	7(0)	6(0)	5(0)	4(0)	5(0)	4(0)	5(0)
ED	97(85)	96(83)	95(80)	73(57)	28(19)	12(4)	6(1)	5(0)	4(1)
C_{2N}	95(81)	93(81)	90(75)	53(34)	19(7)	8(2)	5(0)	5(0)	6(0)
S_3	5(1)	5(1)	6(0)	6(0)	5(0)	4(0)	5(0)	4(0)	5(0)
Simple Scale Alternative (b)									
T _g -NN	62(33)	72(43)	77(47)	99(76)	93(63)	79(45)	98(70)	90(56)	76(43)
M _g -NN	65(38)	74(46)	80(51)	99(78)	94(68)	82(47)	98(70)	90(56)	81(46)
GET	61(33)	71(40)	74(44)	99(75)	86(56)	69(35)	97(68)	83(46)	63(32)
MET	63(36)	72(42)	76(47)	99(76)	91(63)	76(42)	98(68)	90(56)	77(43)
SWR	5(0)	5(0)	5(0)	33(14)	19(7)	13(3)	23(10)	20(5)	12(3)
DM	63(36)	50(21)	32(4)	72(47)	57(34)	43(24)	4(0)	4(0)	4(0)
ED	5(2)	6(1)	6(1)	98(78)	93(69)	83(56)	30(12)	19(8)	18(6)
C_{2N}	73(41)	84(53)	88(57)	73(42)	66(27)	54(11)	5(0)	5(0)	4(0)
S_3	83(54)	90(64)	92(67)	66(42)	49(28)	37(19)	4(0)	4(0)	4(0)
Complex Scale Alternative (c)									
T _g -NN	99(87)	98(86)	98(85)	99(85)	93(70)	82(54)	95(83)	77(60)	61(44)
M _g -NN	96(73)	96(73)	95(72)	97(85)	85(61)	70(39)	95(80)	86(67)	76(55)
GET	84(63)	79(56)	79(56)	90(76)	35(2)	14(1)	96(84)	77(61)	54(38)
MET	78(48)	77(44)	76(46)	81(60)	37(10)	24(1)	94(78)	83(64)	70(50)
SWR	80(61)	84(64)	82(64)	96(84)	97(84)	96(83)	99(92)	98(88)	96(84)
DM	8(0)	6(0)	7(0)	70(46)	70(43)	68(40)	5(0)	5(0)	5(0)
ED	10(2)	10(2)	8(2)	95(72)	97(74)	95(75)	5(1)	6(0)	4(1)
C_{2N}	7(1)	7(1)	7(2)	74(40)	77(27)	75(15)	5(0)	4(0)	6(0)
S_3	8(1)	9(1)	8(1)	67(43)	67(41)	66(39)	5(0)	5(0)	5(0)
Location and Simple Scale mixed Alternative (d)									
T _g -NN	67(40)	70(42)	78(50)	72(51)	54(34)	36(19)	58(41)	46(31)	34(20)
M _g -NN	69(44)	73(46)	80(53)	69(48)	54(34)	37(21)	70(52)	60(43)	47(32)
GET	64(37)	67(39)	76(46)	53(34)	28(13)	12(4)	37(24)	23(14)	16(8)
MET	66(39)	71(43)	77(49)	51(30)	28(12)	16(5)	49(32)	34(20)	28(14)
SWR	5(0)	5(0)	5(0)	13(3)	12(3)	11(3)	20(7)	22(8)	19(6)
DM	66(40)	47(19)	32(5)	14(4)	8(2)	7(1)	5(0)	4(0)	4(0)
ED	9(2)	9(3)	8(2)	60(39)	32(18)	19(6)	6(1)	5(1)	4(1)
C_{2N}	77(44)	83(54)	89(61)	37(16)	16(4)	10(2)	6(0)	5(0)	5(0)
S_3	84(56)	88(63)	92(69)	11(2)	7(1)	6(1)	5(0)	4(0)	4(0)
Location and Complex Scale Mixed Alternative (e)									
T _g -NN	88(68)	81(59)	78(55)	98(87)	95(83)	90(76)	66(50)	50(36)	38(26)
M _g -NN	84(56)	77(50)	74(45)	98(87)	96(84)	92(78)	78(59)	66(48)	54(39)
GET	68(45)	60(37)	54(31)	93(80)	80(64)	57(43)	49(34)	31(20)	20(11)
MET	65(38)	58(30)	53(27)	94(78)	85(67)	67(50)	60(43)	46(29)	34(18)
SWR	47(24)	42(22)	42(21)	65(41)	68(47)	64(43)	29(13)	29(13)	30(13)
DM	8(0)	8(0)	7(0)	3(0)	5(0)	5(0)	5(0)	4(0)	5(0)
ED	40(25)	33(17)	25(12)	90(72)	62(46)	22(15)	6(1)	4(0)	4(1)
C_{2N}	40(20)	28(11)	22(8)	61(40)	22(10)	10(3)	5(0)	5(0)	6(0)
S_3	6(0)	8(1)	6(0)	4(0)	5(0)	5(0)	5(0)	4(0)	5(0)

TABLE 5

The power of the tests under Settings IV-VI with the location alternative (a), the simple scale alternative (b), the complex scale alternative (c), the location and simple scale mixed alternative (d) and the location and complex scale mixed alternative (e) where the nominal significance level $\alpha = 0.05$, for $n = 200$, $\tau = [\frac{n}{3}]$ and $d = 200, 500, 1000$.

	Setting IV (χ^2_5)			Setting V (Gaussian mixture)			Setting VI (Gaussian outlier)		
	200	500	1000	200	500	1000	200	500	1000
Location Alternative (a)									
T _g -NN	73(54)	60(44)	48(32)	30(17)	41(27)	56(41)	59(43)	48(32)	38(22)
M _g -NN	74(56)	65(46)	54(37)	32(18)	42(27)	58(42)	61(44)	50(34)	42(24)
GET	60(43)	46(30)	33(21)	29(17)	39(25)	51(34)	44(30)	30(17)	21(09)
MET	64(47)	52(35)	39(25)	30(18)	41(28)	54(37)	48(33)	34(19)	27(13)
SWR	20(7)	18(6)	15(3)	20(6)	24(9)	31(13)	18(7)	15(4)	13(4)
DM	6(0)	5(0)	5(0)	7(0)	6(0)	7(0)	4(0)	6(0)	7(0)
ED	94(80)	93(79)	91(76)	6(1)	5(1)	6(1)	93(8)	90(73)	87(7)
C_{2N}	95(80)	92(78)	88(73)	87(53)	83(24)	84(11)	78(61)	44(26)	19(06)
S_3	5(1)	4(0)	6(1)	7(0)	6(0)	7(0)	4(0)	4(0)	6(0)
Simple Scale Alternative (b)									
T _g -NN	88(59)	86(56)	82(55)	70(46)	80(54)	88(65)	84(57)	78(48)	71(43)
M _g -NN	90(64)	89(61)	86(58)	71(49)	81(58)	88(69)	84(61)	77(52)	70(47)
GET	85(57)	84(53)	80(51)	65(40)	76(51)	84(60)	87(61)	83(57)	75(51)
MET	88(61)	87(57)	83(54)	66(45)	76(55)	83(64)	85(59)	78(51)	72(44)
SWR	5(1)	6(0)	6(0)	5(0)	5(0)	5(1)	5(0)	5(0)	5(1)
DM	90(65)	82(52)	55(25)	6(0)	5(0)	5(0)	69(50)	59(40)	43(25)
ED	6(1)	8(2)	6(2)	5(1)	4(1)	5(1)	11(4)	13(4)	11(3)
C_{2N}	86(57)	91(63)	91(63)	6(1)	6(1)	6(0)	65(40)	56(31)	42(16)
S_3	93(68)	96(72)	96(72)	6(0)	5(0)	5(0)	53(38)	39(26)	24(14)
Complex Scale Alternative (c)									
T _g -NN	82(67)	72(55)	66(48)	70(53)	61(48)	63(47)	73(52)	67(50)	65(48)
M _g -NN	74(49)	62(36)	58(33)	49(31)	42(28)	47(30)	72(50)	69(50)	66(47)
GET	57(40)	44(26)	37(20)	24(13)	18(9)	21(10)	44(28)	40(25)	37(24)
MET	52(29)	41(20)	36(15)	21(9)	15(6)	17(6)	45(27)	43(26)	44(25)
SWR	64(43)	63(43)	64(42)	92(77)	92(79)	94(81)	58(36)	57(33)	57(34)
DM	4(0)	4(0)	4(0)	5(0)	5(0)	6(0)	5(1)	4(0)	4(0)
ED	8(1)	7(1)	8(1)	5(0)	5(1)	4(1)	8(1)	7(1)	7(0)
C_{2N}	3(0)	4(1)	5(0)	5(0)	5(0)	6(0)	5(0)	5(0)	6(0)
S_3	4(0)	4(0)	5(0)	5(0)	5(0)	6(0)	5(0)	5(0)	5(0)
Location and Simple Scale mixed Alternative (d)									
T _g -NN	67(38)	65(35)	60(33)	70(44)	81(54)	86(61)	90(66)	83(55)	79(49)
M _g -NN	70(42)	67(39)	63(38)	68(45)	81(56)	86(63)	86(62)	78(52)	74(47)
GET	66(37)	62(32)	58(31)	70(45)	81(56)	87(65)	93(71)	86(62)	80(60)
MET	66(39)	66(36)	60(34)	67(44)	79(57)	84(62)	88(64)	81(52)	75(50)
SWR	6(1)	5(0)	6(0)	7(1)	6(1)	7(1)	7(1)	8(2)	9(1)
DM	76(46)	57(27)	34(9)	7(0)	6(0)	6(0)	73(50)	59(37)	44(26)
ED	14(5)	10(3)	8(3)	5(1)	5(1)	4(1)	44(26)	38(22)	37(20)
C_{2N}	73(41)	77(44)	79(46)	52(22)	38(10)	38(5)	76(51)	57(32)	43(22)
S_3	82(54)	85(55)	85(56)	6(0)	6(0)	6(0)	55(38)	36(22)	24(14)
Location and Complex Scale Mixed Alternative (e)									
T _g -NN	59(41)	48(32)	42(26)	53(37)	52(34)	53(39)	82(65)	75(59)	73(57)
M _g -NN	52(30)	41(23)	39(21)	42(25)	40(24)	45(29)	81(64)	76(59)	74(56)
GET	39(22)	25(12)	24(11)	19(9)	19(7)	20(10)	58(42)	49(32)	43(28)
MET	37(16)	26(11)	25(10)	15(6)	16(5)	18(7)	60(41)	52(34)	48(30)
SWR	42(22)	40(21)	40(19)	74(53)	76(54)	79(60)	56(33)	53(32)	50(29)
DM	4(0)	4(0)	5(0)	5(0)	5(0)	5(0)	4(0)	5(0)	4(0)
ED	10(2)	7(1)	7(1)	4(0)	5(1)	6(1)	43(25)	34(19)	28(14)
C_{2N}	8(2)	6(1)	5(0)	8(1)	9(1)	11(1)	20(9)	11(2)	4(0)
S_3	4(0)	4(0)	4(0)	5(0)	5(0)	5(0)	4(0)	6(0)	4(0)

and M_g -NN outperform other methods for the alternatives (b), (c), and (e), while DM, S_3 and C_{2N} are well for the alternative (b) but lose power for the alternatives (b) and (e). For the scale alternative (b), S_3 exhibits the highest power, and T_g and M_g also perform well.

For the Gaussian mixture distribution, C_{2N} has the highest power for the location alternative (a), while T_g -NN and M_g -NN are the second best. For alternatives (b) and (d), T_g -NN and M_g -NN have the best performance, followed immediately by GET and MET, while all other methods have unsatisfactory performance. For alternatives (c) and (e), SWR achieves the highest power, while T_g -NN and M_g -NN are also good with the performance better than other methods.

Finally, for the multivariate normal distribution with t_7 outliers, ED is the best for the location alternative, while for $d = 1000$, it is outperformed by T_g -NN and M_g -NN in the detection accuracy. For other alternatives, T_g -NN and M_g -NN dominate other methods, followed by GET and MET. It shows that T_g -NN and M_g -NN are robust to outliers.

In summary, the distance-based methods ED, C_{2N} , and S_3 , as well as DM, are powerful for the light-tailed distribution. Specifically, ED exhibits superior power for the location alternative, S_3 and DM are more powerful for the simple scale alternative, while C_{2N} covers both the location and the scale alternatives. Nevertheless, these methods suffer from outliers and are less powerful for heavy-tailed distributions. On the contrary, the graph-based methods GET, MET, and SWR are less sensitive to outliers and show good performance for the complex scale alternative. The problem with these methods is that they use less information than distance-based methods, thus suffering from the lack of power for light-tailed distribution and the location alternative. In particular, SWR uses the least information compared to GET and MET, so it has almost no power in many settings and alternatives when other methods attain moderate power. However, T_g -NN and M_g -NN are different from all methods, which possess comparable power for the light-tailed distributions and show robustness for the heavy-tailed distributions and outliers and perform well under a wide range of alternatives.

5. Real Data Examples

5.1. Seizure Detection from Functional Connectivity Networks

We illustrate RING-CPD for the identification of epileptic seizures, which over two million Americans are suffering from (Iasemidis, 2003). As a promising therapy, responsive neurostimulation requires automated algorithms to detect seizures as early as possible. Besides, to identify seizures, physicians have to review abundant electro-encephalogram (EEG) recordings, which in some patients may be quite subtle. Hence, it is important to develop methods with low false positive and false negative rates to detect seizures from the EEG recordings. We use the “Detect seizures in intracranial EEG (iEEG) recordings” database

by the UPenn and Mayo Clinic (<https://www.kaggle.com/c/seizure-detection>), which consists of the EEG recordings of 12 subjects (eight patients and four dogs). For each subject, both the normal brain activity and the seizure activity are recorded multiple times, which are one-second clips with various channels (from 16 to 72), reducing to a multivariate stream of iEEGs. Following the procedure of [Zambon, Alippi and Livi \(2019\)](#), we represent the iEEG data as functional connectivity networks using Pearson correlation in the high-gamma band (70-100Hz) ([Bastos and Schoffelen, 2016](#)). Functional connectivity networks are weighted graphs, where the vertexes are the electrodes, and the weights of edges correspond to the coupling strength of the vertexes. An illustration of the networks is in Figure 4. The sample sizes of the 12 subjects are also different, and the true change-point τ 's are also known - before the change-point, the networks are generated from the seizure period, while after the change-point, the networks are generated from the normal brain activity.

We do not compare SWR here since SWR does not perform well in the simulation studies and is time-consuming. Besides, C_{2N} is not only time-consuming but also memory-consuming (e.g., it requires at least 17Gb size of memory when $n = 1320$); we are only able to run it for $n \leq 600$, thus only showing its result for dog 1, and patients 1 and 4. We use the Frobenius norm to measure the distance between the observations represented by the weighted adjacency graphs. Since the sample size of each subject is large enough, we use the asymptotic p -value approximation for M_g -NN and MET. We omit the result of T_g -NN and GET since their p -value approximations are not as exact as M_g -NN and MET, respectively. For DM, ED and S_3 , we still use 1,000 permutations to obtain the p -values. The results are summarized in Table 6, where the absolute difference between the true change-point and the detected change-point $|\hat{\tau} - \tau|$ is reported. The p -values are not reported as they are smaller than 0.01 for all methods and subjects. Our method achieves the same detection error as MET, which is very small for all subjects. ED also performs well, although DM and S_3 achieve small errors for most subjects but attain large detection errors for patients 3 and 4. The performance of C_{2N} is not robust in that it shows a large detection error for patient 4.

5.2. *Changed Interval Detection for New York Taxi Data*

We then illustrate our methods for changed interval detection on the travel pattern in New York Central Park. We use the public dataset on the NYC Taxi and Limousine Commission (TLC) website (<https://www1.nyc.gov/site/tlc/about/tlc-trip-record-data.page>). We use the yellow taxi trip records in the year 2014, which contain the city's taxi pickup and drop-off times (date) and locations (longitude and latitude coordinates). We set the latitude range of New York Central Park as 40.77 to 40.79 and the longitude range as -73.97 to -73.96. The boundary of New York City is set as 40.67 to 41.82 in latitude and -74.02 to -73.86. We only consider those trips that began with a pickup in New York City and ended with a drop-off in New York Central Park. To represent the

TABLE 6
The absolute difference between the true change-point and the detected change-point ($|\hat{\tau} - \tau|$). The p-values of all methods for all subjects are smaller than 05.

Subject	n	τ	M_g -NN	MET	DM	ED	C_{2N}	S_3
Dog 1	596	178	0	0	0	1	0	0
Dog 2	1320	172	4	4	1	3	-	1
Dog 3	5240	480	0	0	1	1	-	1
Dog 4	3047	257	3	3	3	2	-	3
Patient 1	174	70	1	1	1	0	7	1
Patient 2	3141	151	7	7	13	1	-	13
Patient 3	1041	327	0	0	162	1	-	162
Patient 4	210	20	0	0	67	11	137	67
Patient 5	2745	135	3	3	5	2	-	5
Patient 6	2997	225	0	0	0	1	-	0
Patient 7	3521	282	2	2	3	4	-	3
Patient 8	1890	180	0	0	0	1	-	0

travel pattern of each day, we split the New York City into a 30×30 grid with equal size cells. Then we represent each day by a 30×30 matrix, whose elements are the numbers of taxi pickups in the corresponding cells. We use the Frobenius norm to construct the similarity graphs in the subsequent analysis. The p -values of all methods are obtained through 1000 permutations.

We first compare our methods with GET and MET. We set $l_0 = \max\{5, [0.05n]\}$ and $l_1 = n - l_0$. The significance level α is set as 0.05. All methods detect the same changed interval 06/17-09/02 with p -values < 0.001 , which almost overlaps totally with the summer break.

Since there may be multiple changed intervals, we apply the methods sequentially. Specifically, we apply the methods to the three segments divided by the detected changed interval. All methods report p -values < 0.05 for the three segments. In the period 01/01-06/16, the four methods all detect the changed interval 03/21-04/02, which is around the spring break of most American universities. In the period 06/17-09/02, GET and MET detect the changed interval 07/03-09/02, while T_g -NN and M_g -NN detect the changed interval 07/01-09/02, both of them covers the Independence Day. T_g -NN and M_g -NN are more significant than GET and MET with p -values < 0.001 . In the period 09/03-12/31, the four methods detect the changed interval 11/14-12/31, which is around the beginning day of the fall term/quarter to the midterm, and 11/14 is about ten days before the Thanksgiving day.

We further perform the four methods in the segments longer than 40 days. The only detected changed interval is 12/25-12/30 in the segment 11/14-12/31, which is the week of Christmas where GET, T_g -NN and M_g -NN report p -values < 0.05 , but MET reports the p -value = 0.054. Finally, we apply the methods to the period 11/14-12/14, and no changed interval is detected anymore. The result is summarized in Table 7.

We then show the performance of other methods. Since both ED and S_3 can detect multiple change-points, we apply them directly to the whole sequence 01/01-12/31. We also compare with C_{2N} . Although C_{2N} is not designed for multiple change-points detection, we can apply it sequentially similarly to the

TABLE 7
The detected changed intervals and corresponding p -values of T_g -NN, M_g -NN, GET and MET for the NYC taxi data.

Time period	T_g -NN	M_g -NN	GET	MET	Nearby Events
01/01-12/31		06/17-09/02			
p -value	< 0.001	< 0.001	< 0.001	< 0.001	Summer break
01/01-06/16		03/21-04/02			
p -value	< 0.001	< 0.001	< 0.001	< 0.001	Spring break
06/17-09/02	07/01-09/02	07/01-09/02	07/03-09/02	07/03-09/02	Independence Day
p -value	< 0.001	< 0.001	0.009	0.015	
09/03-12/31		11/14-12/31			
p -value	0.001	< 0.001	< 0.001	< 0.001	Thanksgiving
01/01-03/20	02/12-02/16	02/12-02/16	03/01-03/05	02/12-02/16	-
p -value	0.263	0.279	0.384	0.352	
04/03-06/16	05/03-05/07	05/03-05/07	05/03-05/07	04/05-04/09	-
p -value	0.101	0.110	0.471	0.529	
07/01-09/02	07/07-08/15	07/07-08/15	07/07-08/15	07/07-08/15	-
p -value	0.062	0.051	0.209	0.207	
09/03-11/13	09/06-11/13	09/06-11/13	09/22-09/27	09/22-09/27	-
p -value	0.102	0.088	0.108	0.096	
11/14-12/31		12/25-12/30			
p -value	0.029	0.028	0.038	0.054	Christmas
11/14-12/24	11/27-12/01	11/27-12/01	11/27-12/01	11/27-12/01	-
p -value	0.152	0.249	0.115	0.215	

TABLE 8
The detected change-points and corresponding p -values of ED, S_3 and C_{2N} for the NYC taxi data.

Method				
ED	CP	04/05	06/18	09/09
	p -values	0.029	0.001	0.001
S_3	CP	07/04	07/11	09/02
	p -values	0.003	0.035	< 0.001
C_{2N}	CP	01/03	06/17	08/22
	p -values	0.014	< 0.001	0.025
			< 0.001	0.006
				12/25

above procedure, which is the binary segmentation procedure also used by [Nie and Nicolae \(2021\)](#).

ED detects three change-points 04/05, 06/18 and 09/09 with p -values 0.029, 0.001 and 0.001, respectively. S_3 detects four change-points, which are 07/04, 07/11, 09/02, and 12/25, with p -values 0.003, 0.035, < 0.001 and < 0.001, respectively. C_{2N} detects five change-points, which are 01/03, 06/17, 08/22, 09/02, and 12/25, with p -values 0.014, < 0.001, 0.025, < 0.001 and 0.006. The result is summarized in Table 8.

To further validate the results, we plot the distance matrix of the whole year in Figure 5 (a). It is obvious that there are two changes around the days 80-90, 175 to 250, which match the changed intervals of spring break and summer break. We further plot the distance matrices of the three segments divided by the first changed interval detected by our methods, which are presented in Figure 5 (b), (c), and (d), respectively. The detected changed intervals by our methods and MET and GET can be observed from distance matrices clearly,

which verifies the conclusion. As a result, our methods can detect more changed intervals in New York taxi data compared to ED, C_{2N} and S_3 , and are more significant than GET and MET for some detected changed intervals.

6. Discussion

6.1. Kernel and Distance IN Graph CPD

The approach proposed in this paper can also be extended to other frameworks using different methods to weight the similarity graphs. For example, kernel-based CPD methods are popular since they can be applied to any data and distance-based methods are intuitive. However, the existing kernel-based methods and distance-based methods can not provide the fast type I error control or can not guarantee localization accuracy. Our approach provides a possible way to incorporate the kernel or distance by the following Kernel IN by Graph Change-Point Detection (KING-CPD) and Distance IN by Graph Change-Point Detection (DING-CPD) methods. Specifically, we can use the kernel values or (negative) pairwise distances to weight the similarity graphs, and the asymptotic property still holds under mild conditions. Let

$$K_{ij} = K(y_i, y_j) \mathbb{1}((i, j) \in G_k),$$

where K is a kernel function or a negative distance function, for example, the Gaussian kernel $K(y_i, y_j) = \exp(-\|y_i - y_j\|^2/(2\sigma^2))$ with the kernel bandwidth σ or the negative l_1 distance $K(y_i, y_j) = -\|y_i - y_j\|_1$, and G_k is a similarity graph such as the k -NNG and the k -MST. We require Condition 7 which essentially states that there is no element of R_{ij} dominates others.

$$\text{Condition 7. } \max_{i,j} K_{ij} = o(n^2 r_d^2).$$

Theorem 6.1. *Replacing R_{ij} by K_{ij} in Conditions 1-6, and the definition of Z_{diff} and Z_w , then under Conditions 1-7, we have*

1. $\{Z_{\text{diff}}(\lfloor nu \rfloor) : 0 < u < 1\}$ and $\{Z_w(\lfloor nu \rfloor) : 0 < u < 1\}$ converge to independent Gaussian processes in finite dimensional distributions, which we denote as $\{Z_{\text{diff}}^*(u) : 0 < u < 1\}$ and $\{Z_w^*(u) : 0 < u < 1\}$, respectively.
2. $\{Z_{\text{diff}}(\lfloor nu \rfloor, \lfloor nv \rfloor) : 0 < u < v < 1\}$ and $\{Z_w(\lfloor nu \rfloor, \lfloor nv \rfloor) : 0 < u < v < 1\}$ converge to independent two-dimension Gaussian random fields in finite dimensional distributions, which we denote as $\{Z_{\text{diff}}^*(u, v) : 0 < u < v < 1\}$ and $\{Z_w^*(u, v) : 0 < u < v < 1\}$, respectively.

Besides, Theorem 3.2 also holds by replacing R_{ij} by K_{ij} .

The proof of Theorem 6.1 follows straightforwardly from the proof of Theorems 3.1 and 3.2, thus omitted here.

6.2. Computational Efficiency

Another important property of RING-CPD is the potential computational efficiency by avoiding computing the pairwise distance of the n observations, which has a computational complexity of $O(dn^2)$ for d -dimensional data. Specifically, if the approximate k -NNG (Beygelzimer et al., 2019) is used for RING-CPD, the computational complexity is $O(dn(\log n + k \log d) + nk^2)$, which is usually faster than $O(dn^2)$. A detailed discussion of the procedure and time complexity can be found in Liu and Chen (2020).

6.3. Conclusion

In this paper, we introduce the new rank-based approach RING-CPD for single change-point detection and changed interval detection. For the choice of the graph, when the sample size n is small, we recommend k -NNG with $k = [n^{0.65}]$ based on its robust performance; when n is large, it may be sufficient to use $k = 10$ to achieve adequate power considering the computational efficiency. Both T_g -NN and M_g -NN work well for various alternatives with similar performance. We suggest using M_g -NN based on its accurate finite sample approximation to the asymptotic distribution, thus enabling a fast and accurate control of type I error. Although the proposed method is designed for single change-point and changed interval detection, it can be easily extended to find multiple change-points similarly to Zhang and Chen (2021), using the idea of wild binary segmentation (Fryzlewicz, 2014) or seeded binary segmentation (Kovács et al., 2020).

Funding

The authors were partly supported by NSF Grant DMS-1848579.

References

ARLOT, S., CELISSE, A. and HARCHAOUI, Z. (2019). A kernel multiple change-point algorithm via model selection. *Journal of machine learning research* **20**.

BAI, J. and PERRON, P. (1998). Estimating and testing linear models with multiple structural changes. *Econometrica* 47–78.

BARNETT, I. and ONNELA, J.-P. (2016). Change point detection in correlation networks. *Scientific reports* **6** 1–11.

BASTOS, A. M. and SCHOFFELEN, J.-M. (2016). A tutorial review of functional connectivity analysis methods and their interpretational pitfalls. *Frontiers in systems neuroscience* **9** 175.

BEYGELZIMER, A., KAKADET, S., LANGFORD, J., ARYA, S., MOUNT, D. and LI, S. (2019). Fast Nearest Neighbor Search Algorithms and Applications. *FNN: kd-tree fast k-nearest neighbor search algorithms*.

BHATTACHARYYA, G. K. and JOHNSON, R. A. (1968). Nonparametric tests for shift at an unknown time point. *The Annals of Mathematical Statistics* **39** 1731–1743.

CHANG, W.-C., LI, C.-L., YANG, Y. and PÓCZOS, B. (2019). Kernel change-point detection with auxiliary deep generative models. *arXiv preprint arXiv:1901.06077*.

CHEN, H. (2019). Change-point detection for multivariate and non-euclidean data with local dependency. *arXiv preprint arXiv:1903.01598*.

CHEN, H., CHEN, X. and SU, Y. (2018). A weighted edge-count two-sample test for multivariate and object data. *Journal of the American Statistical Association* **113** 1146–1155.

CHEN, H. and FRIEDMAN, J. H. (2017). A new graph-based two-sample test for multivariate and object data. *Journal of the American statistical association* **112** 397–409.

CHEN, J. and GUPTA, A. K. (2012). Parametric statistical change point analysis: with applications to genetics, medicine, and finance.

CHEN, H. and ZHANG, N. (2015). Graph-based change-point detection. *The Annals of Statistics* **43** 139–176.

CHENOURI, S., MOZAFFARI, A. and RICE, G. (2020). Robust multivariate change point analysis based on data depth. *Canadian Journal of Statistics* **48** 417–446.

CHU, L. and CHEN, H. (2019). Asymptotic distribution-free change-point detection for multivariate and non-euclidean data. *The Annals of Statistics* **47** 382–414.

DARKHOVSKH, B. (1976). A nonparametric method for the a posteriori detection of the “disorder” time of a sequence of independent random variables. *Theory of Probability & Its Applications* **21** 178–183.

DESOBRY, F., DAVY, M. and DONCARLI, C. (2005). An online kernel change detection algorithm. *IEEE Transactions on Signal Processing* **53** 2961–2974.

DUBEY, P. and MÜLLER, H.-G. (2020). Fréchet Change Point Detection.

EAGLE, N., PENTLAND, A. S. and LAZER, D. (2009). Inferring friendship network structure by using mobile phone data. *Proceedings of the national academy of sciences* **106** 15274–15278.

FRIEDMAN, J. H. and RAFSKY, L. C. (1979). Multivariate generalizations of the Wald-Wolfowitz and Smirnov two-sample tests. *The Annals of Statistics* **7** 697–717.

FRYZLEWICZ, P. (2014). Wild binary segmentation for multiple change-point detection. *The Annals of Statistics* **42** 2243–2281.

GARREAU, D. and ARLOT, S. (2018). Consistent change-point detection with kernels. *Electronic Journal of Statistics* **12** 4440–4486.

GERSTENBERGER, C. (2018). Robust Wilcoxon-Type Estimation of Change-Point Location Under Short-Range Dependence. *Journal of Time Series Analysis* **39** 90–104.

HENZE, N. (1988). A multivariate two-sample test based on the number of nearest neighbor type coincidences. *The Annals of Statistics* **16** 772–783.

IASEMIDIS, L. D. (2003). Epileptic seizure prediction and control. *IEEE Transactions on Neural Networks* **14** 101–107.

actions on Biomedical Engineering **50** 549–558.

KOSSINETS, G. and WATTS, D. J. (2006). Empirical analysis of an evolving social network. *science* **311** 88–90.

KOVÁCS, S., LI, H., BÜHLMANN, P. and MUNK, A. (2020). Seeded binary segmentation: A general methodology for fast and optimal change point detection. *arXiv preprint arXiv:2002.06633*.

LI, J. (2020). Asymptotic distribution-free change-point detection based on interpoint distances for high-dimensional data. *Journal of Nonparametric Statistics* **32** 157–184.

LI, S., XIE, Y., DAI, H. and SONG, L. (2015). M-statistic for kernel change-point detection. *Advances in Neural Information Processing Systems* **28**.

LIU, Y.-W. and CHEN, H. (2020). A fast and efficient change-point detection framework for modern data. *arXiv preprint arXiv:2006.13450*.

LOMBARD, F. (1983). Asymptotic distributions of rank statistics in the change-point problem. *South African Statistical Journal* **17** 83–105.

LOMBARD, F. (1987). Rank tests for changepoint problems. *Biometrika* **74** 615–624.

LUNG-YUT-FONG, A., LÉVY-LEDUC, C. and CAPPÉ, O. (2015). Homogeneity and change-point detection tests for multivariate data using rank statistics. *Journal de la Société Française de Statistique* **156** 133–162.

MALLADI, R., KALAMANGALAM, G. P. and AAZHANG, B. (2013). Online Bayesian change point detection algorithms for segmentation of epileptic activity. In *2013 Asilomar conference on signals, systems and computers* 1833–1837. IEEE.

MATTESON, D. S. and JAMES, N. A. (2014). A nonparametric approach for multiple change point analysis of multivariate data. *Journal of the American Statistical Association* **109** 334–345.

NIE, L. and NICOLAE, D. L. (2021). Weighted-Graph-Based Change Point Detection. *arXiv preprint arXiv:2103.02680*.

PAGE, E. S. (1954). Continuous inspection schemes. *Biometrika* **41** 100–115.

PEEL, L. and CLAUSET, A. (2015). Detecting change points in the large-scale structure of evolving networks. In *Twenty-Ninth AAAI Conference on Artificial Intelligence*.

PETTITT, A. N. (1979). A non-parametric approach to the change-point problem. *Journal of the Royal Statistical Society: Series C (Applied Statistics)* **28** 126–135.

SCHECHTMAN, E. (1982). A nonparametric test for detecting changes in location. *Communications in Statistics-Theory and Methods* **11** 1475–1482.

SCHILLING, M. F. (1986). Multivariate two-sample tests based on nearest neighbors. *Journal of the American Statistical Association* **81** 799–806.

SHI, X., WU, Y. and RAO, C. R. (2017). Consistent and powerful graph-based change-point test for high-dimensional data. *Proceedings of the National Academy of Sciences* **114** 3873–3878.

SHU, L., CHEN, Y., ZHANG, W. and WANG, X. (2022). Spatial rank-based high-dimensional change point detection via random integration. *Journal of Multivariate Analysis* **189** 104942.

SIEGMUND, D. and YAKIR, B. (2007). *The statistics of gene mapping*. Springer Science & Business Media.

SIEGMUND, D., YAKIR, B. and ZHANG, N. R. (2011). Detecting simultaneous variant intervals in aligned sequences. *The Annals of Applied Statistics* **5** 645–668.

SONG, H. and CHEN, H. (2020). Asymptotic distribution-free change-point detection for data with repeated observations. *arXiv preprint arXiv:2006.10305*.

SRIVASTAVA, M. and WORSLEY, K. J. (1986). Likelihood ratio tests for a change in the multivariate normal mean. *Journal of the American Statistical Association* **81** 199–204.

STAUDACHER, M., TELSER, S., AMANN, A., HINTERHUBER, H. and RITSCHMARTE, M. (2005). A new method for change-point detection developed for on-line analysis of the heart beat variability during sleep. *Physica A: Statistical Mechanics and its Applications* **349** 582–596.

TALIH, M. and HENGARTNER, N. (2005). Structural learning with time-varying components: tracking the cross-section of financial time series. *Journal of the Royal Statistical Society: Series B (Statistical Methodology)* **67** 321–341.

WANG, Y., WANG, Z. and ZI, X. (2020). Rank-based multiple change-point detection. *Communications in Statistics-Theory and Methods* **49** 3438–3454.

WANG, G., ZOU, C. and YIN, G. (2018). Change-point detection in multinomial data with a large number of categories. *The Annals of Statistics* **46** 2020–2044.

ZAMBON, D., ALIPPI, C. and LIVI, L. (2019). Change-point methods on a sequence of graphs. *IEEE Transactions on Signal Processing* **67** 6327–6341.

ZHANG, J. and CHEN, H. (2017). Graph-Based Two-Sample Tests for Data with Repeated Observations. *arXiv preprint arXiv:1711.04349*.

ZHANG, J. and CHEN, H. (2020). Graph-Based Two-Sample Tests for Data with Repeated Observations. *Statistica Sinica* DOI:10.5705/ss.202019.0116.

ZHANG, C., CHEN, N. and WU, J. (2020). Spatial rank-based high-dimensional monitoring through random projection. *Journal of Quality Technology* **52** 111–127.

ZHANG, Y. and CHEN, H. (2021). Graph-based multiple change-point detection. *arXiv preprint arXiv:2110.01170*.

ZHANG, N. R., SIEGMUND, D. O., JI, H. and LI, J. Z. (2010). Detecting simultaneous changepoints in multiple sequences. *Biometrika* **97** 631–645.

ZHOU, D. and CHEN, H. (2021). RISE: Rank in Similarity Graph Edge-Count Two-Sample Test. *arXiv preprint arXiv:2011.06127*.

ZHU, Y. and CHEN, H. (2021). Limiting Distributions of Graph-based Test Statistics. *arXiv preprint arXiv:2011.06127*.

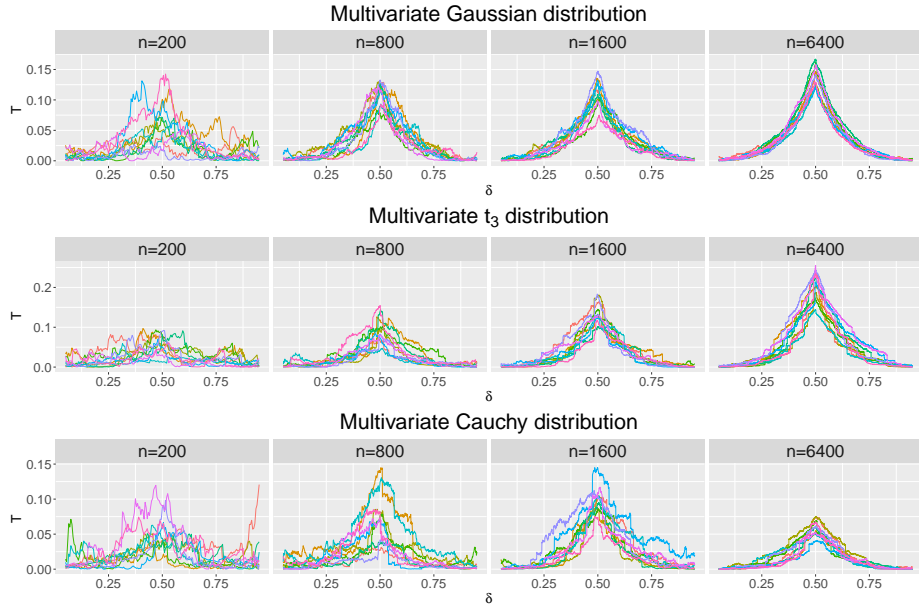


Fig 1: Ten independent sequences (represented by different colors) of $T_R([\delta n])/n$ against δ for $n = 200, 800, 1600$ and 6400 for the three settings.

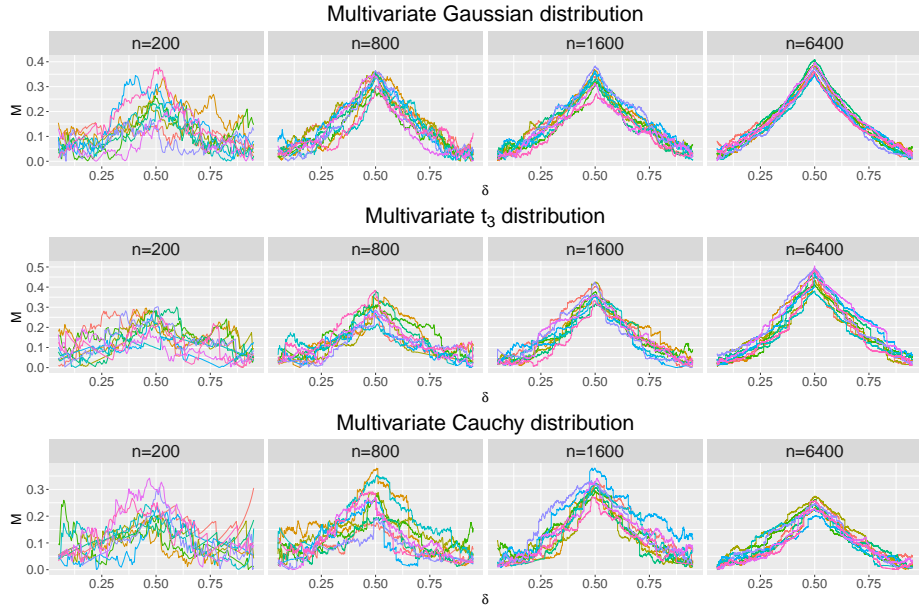


Fig 2: Ten independent sequences (represented by different colors) of $M_R([\delta n])/\sqrt{n}$ against δ for $n = 200, 800, 1600$ and 6400 for the three settings.

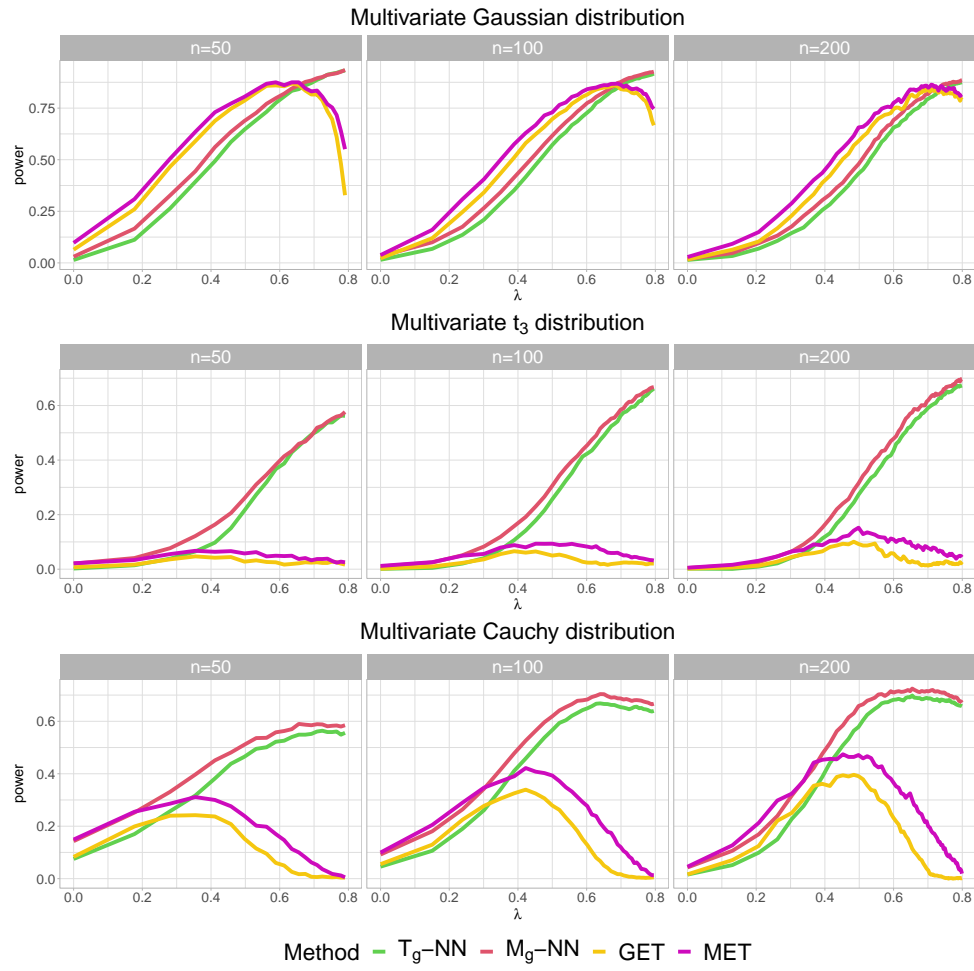


Fig 3: Estimated power of T_g-NN, M_g-NN, GET, and MET over 1000 times of repetitions under each setting.

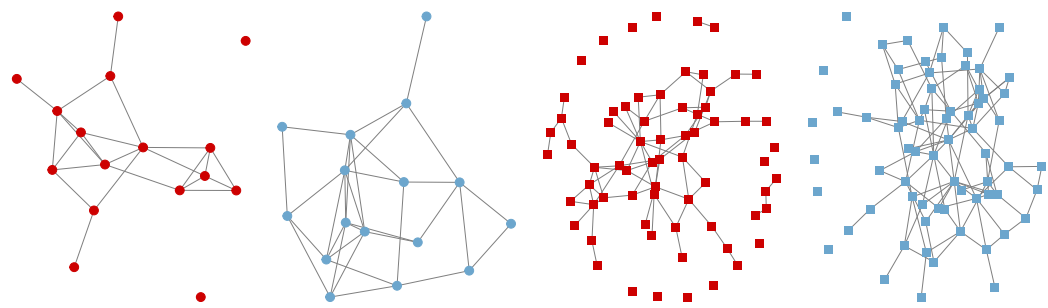


Fig 4: The functional connectivity networks of a dog (circle) and a human (square) during the period of seizure (red) and the normal period (blue). The networks are drawn by only keeping the edges with weights larger than 0.2.

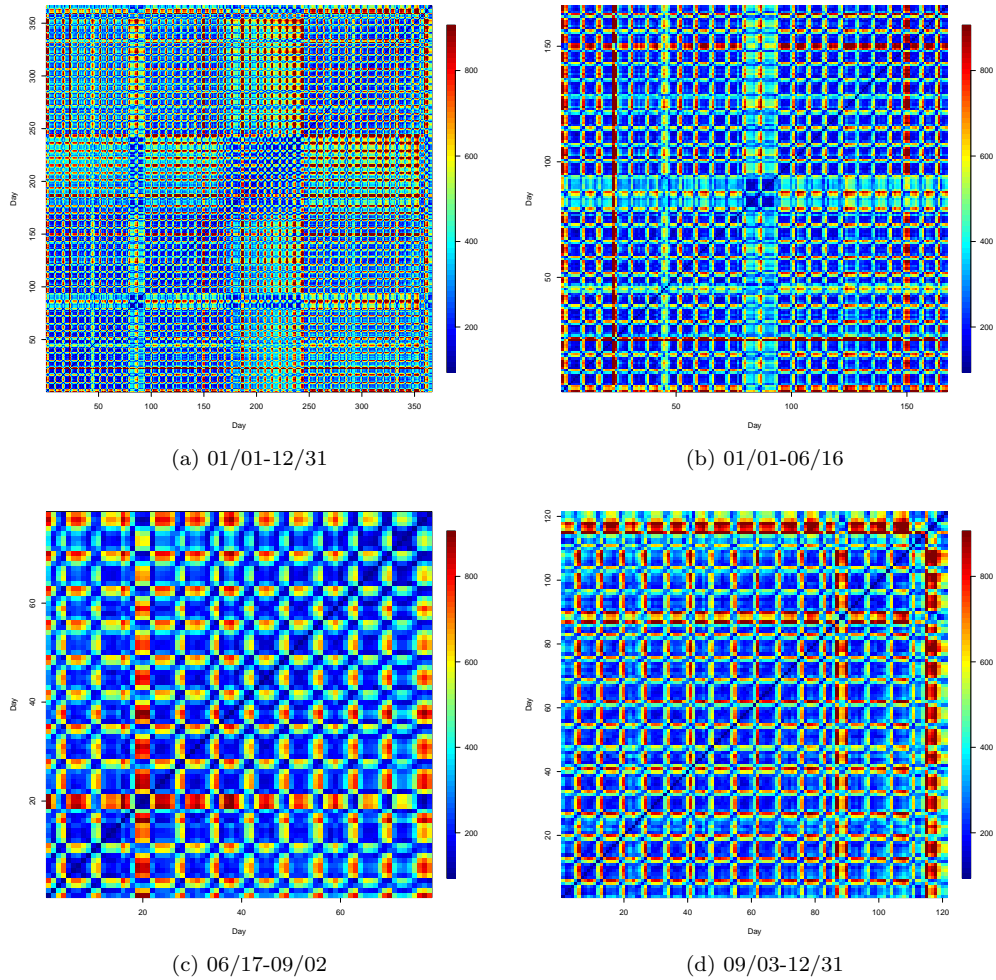


Fig 5: (a) The heat map of the distance matrix of days from 01/01-12/31. (b) The heat map of the distance matrix of days from 01/01-06/16. (c) The heat map of the distance matrix of days from 06/17-09/02. (d) The heat map of the distance matrix of days from 09/03-12/31.